

# **REFINEMENT, CALIBRATION, AND FIELD STUDIES INVOLVING TRANSPORTABLE AEROSOL TIME-OF- FLIGHT MASS SPECTROMETERS**

Final Report (Contract 96-307)  
Prepared for the California Air Resources Board and the California  
Environmental Protection Agency  
Final Version: August 19, 2003

Sylvia H. Pastor<sup>1</sup> and Kimberly A. Prather<sup>2</sup>

<sup>1</sup>Department of Chemistry  
University of California – Riverside  
Riverside, CA 92521

<sup>2</sup>Department of Chemistry and Biochemistry  
Scripps Institution of Oceanography  
9500 Gilman Drive  
University of California  
La Jolla, CA 92093-0314

## **Disclaimer**

---

The statements and conclusions in this Report are those of the contractor and not necessarily those of the California Air Resources Board. The mention of commercial products, their source, or their use in connection with material reported herein is not to be construed as actual or implied endorsement of such products.

## Acknowledgements

---

The authors of this final report would like to thank a number of people who made these studies possible. First of all, in order to keep three newly developed instruments running full time for over 3 months, this obviously took a great deal of group coordination and effort. We would like to acknowledge the entire Prather group for their dedicated participation in the 1997 Southern California Ozone Study – North American Research Strategy for Tropospheric Ozone (SCOS97-NARSTO) during the summer of 1997. For the data analysis and quantification sections, we would like to specifically acknowledge Professor Phillip Hopke and his research group, Dr. Prakash Bhave, Professor Michael Kleeman, Dr. David Ferguson, and Professor Jon Allen for all of their input and guidance. Special acknowledgement is made to the late Professor Glen Cass who without his support and guidance this study and many of the major advances in single particle mass spectrometry would not have been possible. His untimely death is a major loss to us all, both personally as well as professionally.

This report was submitted in fulfillment of Contract 96-307 by U.C. Riverside under the sponsorship of the California Air Resources Board. Work was completed as of April 2001.

# Table of Contents

---

|   |    |
|---|----|
| <b>1. Introduction</b>  |    |
| 1.1. Background on southern California aerosol particles  | 1  |
| 1.2. SCOS97-NARSTO Aerosol Program  | 2  |
| 1.2.1. Riverside aerosol characterization   | 5  |
| 1.2.2. Los Angeles-Azusa aerosol evolution  | 5  |
| 1.2.3. Source characterization  | 5  |
| 1.2.4. Mira Loma and Nitrate-Oriented Trajectory  | 6  |
| 1.2.5. Trends in the Riverside Aerosol  | 7  |
| 1.3. Air Quality during the SCOS97-NARSTO Sampling Period   | 7  |
| <b>2. Riverside Aerosol Characterization</b>  |    |
| 2.1. Overview   | 9  |
| 2.2. Experimental methods   | 10 |
| 2.3. Results and Discussion   | 13 |
| 2.3.1. ART-2a Analysis of ATOFMS Data from August 21-23, 1997   | 13 |
| 2.3.2. Chemical Composition of the Particle Classes Determined by ART-2a Analysis                                     | 15 |
| 2.3.3. Size Distributions of Particle Classes Determined by ART-2a  | 19 |
| 2.3.4. Temporal Characteristics of Riverside Air Quality  | 22 |
| 2.3.5. Scaled Size Distributions with Particle Composition  | 29 |
| 2.4. Conclusions  | 32 |
| <b>3. LA-Azusa Aerosol Evolution</b>  |    |
| 3.1. Introduction   | 33 |
| 3.2. Experimental methods   | 33 |
| 3.3. Results and Discussion   | 34 |
| 3.3.1. Air Mass Trajectories for Transport from Los Angeles to Azusa  | 34 |
| 3.3.2. Chemical Composition Overview Using Digital Mass Spectra for Trajectory 1                                      | 34 |
| 3.3.3. Chemical Class Comparison to Riverside   | 37 |
| 3.3.4. Chemical Composition Overview Using “Stacked” Digital Mass Spectra for Trajectory 1                            | 43 |
| 3.3.5. Dual ion ART-2a Analysis with Higher Vigilance Factor for Trajectory 1   | 46 |
| 3.3.6. Nitrate Enrichment during Trajectory 2 Air Mass Transport  | 52 |
| 3.4. Conclusions  | 57 |
| <b>4. Source Characterization</b>   |    |
| 4.1. Introduction   | 59 |
| 4.2. Experimental methods   | 59 |
| 4.3. Results and Discussion   | 61 |
| 4.3.1. Positive ion ART-2a of Dynamometer Source Particles and Chemical Class Comparison to Riverside Ambient         | 61 |
| 4.3.2. Dual ion ART-2a of Dynamometer Source Particles and Chemical Class Comparison to Los Angeles and Azusa Ambient | 72 |
| 4.4. Conclusions  | 79 |

|   |            |
|---|------------|
| <b>5. Mira Loma Aerosol and Nitrate-Oriented Trajectory</b>   |            |
| 5.1. Introduction   | 81         |
| 5.2. Experimental methods   | 81         |
| 5.3. Results and Discussion   | 82         |
| 5.3.1. Mira Loma Single Particle Composition and Comparison to<br>Riverside Ambient Positive ion ART-2a Classes | 82         |
| 5.3.2. Particle Composition along the Diamond Bar-Mira Loma-<br>Riverside Trajectory                            | 90         |
| 5.3.3. Particle Transformations in Diamond Bar, Mira Loma,<br>And Riverside during Trajectory 3                 | 103        |
| 5.4. Conclusions  | 108        |
| <b>6. Trends in Riverside Aerosol</b>   |            |
| 6.1. Introduction   | 110        |
| 6.2. Experimental methods   | 110        |
| 6.3. Results and Discussion   | 110        |
| 6.3.1. Composition and Size Characteristics of Ambient<br>Riverside Particles                                   | 110        |
| 6.3.2. Temporal Trends of Riverside Particle Classes  | 113        |
| 6.3.3. Composition of Ambient Particles- Matching to Car<br>And Diesel  | 125        |
| 6.4. Conclusions  | 130        |
| <b>7. Establishing ATOFMS quantitation procedures</b>   |            |
| 7.3. Introduction   | 132        |
| 7.4. Experimental methods   | 132        |
| 7.5. Results and Discussion   | 134        |
| 7.3.1. Aerosol Mass Concentration   | 134        |
| 7.3.2. Ammonium and Nitrate Concentration   | 139        |
| 7.6. Conclusions  | 142        |
| <br>Summary and Conclusions.....  | <b>143</b> |
| <br>Recommendations.....  | <b>143</b> |
| <br>Glossary of terms.....  | <b>145</b> |
| <br>List of Appendices.....   | <b>146</b> |
| <br>References.....   | <b>148</b> |

## List of Figures

---

- 1.1 Map of ATOFMS sampling sites for SCOS97-NARSTO.
- 1.2 Daily maximum one-hour TEOM PM<sub>10</sub> and ozone concentrations during SCOS97-NARSTO in Riverside, CA. Adapted from Fujita et al, 1999 (Volume III).
- 2.1 Number of particles per class, identified by ART-2a (vigilance, 0.5; learning 0.05; 20 iterations). Particles sampled by the lab-based ATOFMS in Riverside, CA on August 21-23, 1997.
- 2.2 Normalized weight vectors for common organic particle classes identified by ART-2a: (a) cluster 11 organic carbon with amines I, (b) cluster 4 organic carbon with amines II, (c) cluster 16 elemental carbon I, (d) cluster 17 elemental carbon II, (e) cluster 8 ammonium nitrate I, (f) cluster 13 ammonium nitrate II, (g) cluster 12 ammonium nitrate III, and (h) cluster 14 vanadium-rich.
- 2.3 Normalized weight vectors for common inorganic particle classes identified by ART-2a: (a) cluster 1 sea salt I, (b) cluster 2 sea salt II, (c) cluster 3 calcium-rich I, (d) cluster 6 calcium-rich II, (e) cluster 15 iron-rich, (f) cluster 5 potassium-rich I, (g) cluster 7 potassium-rich II, and (h) cluster 9 potassium-rich III.
- 2.4 Normalized weight vectors for common soil dust particle classes identified by ART-2a: (a) cluster 10, (b) cluster 18, (c) cluster 19, and (d) cluster 20.
- 2.5 Similarity plot for weight matrices from Riverside ambient and itself (vigilance factor 0.5).
- 2.6 Size distribution plots for common organic particle classes identified by ART-2a: (a) cluster 11 organic carbon with amines I, (b) cluster 4 organic carbon with amines II, (c) grouped clusters 16 and 17 elemental carbon, (d) cluster 14 vanadium-rich (e) cluster 8 ammonium nitrate I, (f) cluster 13 ammonium nitrate II, and (g) cluster 12 ammonium nitrate III.
- 2.7 Size distribution plots for common inorganic particle classes identified by ART-2a: (a) cluster 1 sea salt I, (b) cluster 2 sea salt II, (c) cluster 3 calcium-rich I, (d) cluster 6 calcium-rich II, (e) cluster 15 iron-rich, (f) grouped clusters 5 and 7 potassium-rich, (g) cluster 9 potassium-rich III, and (h) grouped clusters 10, 18, 19, and 20 soil dust.
- 2.8 Time series plots for hourly ozone, PM<sub>10</sub>, and b<sub>scat</sub> measurements for Riverside, August 21-23, 1997 (note the two y-axes).
- 2.9 Representative air parcel trajectory arriving at Riverside, CA during elevated PM<sub>10</sub> at: (a) 7:00 August 21, 1997, (b) 8:00 August 22, 1997, (c) 8:00 August 23, 1997, and elevated ozone at: (d) 16:00 August 21, 1997 (d) 17:00 August 22, 1997(d) 13:00 August 23, 1997.
- 2.10 Time series plots of common organic particle classes identified by ART-2a: (a) cluster 11 organic carbon with amines I, (b) cluster 4 organic carbon with amines II, (c) grouped clusters 16 and 17 elemental carbon, (d) cluster 14 vanadium-rich, (e) cluster 8 ammonium nitrate I, (f) cluster 13 ammonium nitrate II, and (g) cluster 12 ammonium

- nitrate III with the temporal trend ozone overlaid. Temporal resolution is 30 min for the single particle data and 60 min for the ozone data.
- 2.11 Time series plots for common inorganic particle classes identified by ART-2a: (a) cluster 1 sea salt I, (b) cluster 2 sea salt II, (c) cluster 3 calcium-rich I, (d) cluster 6 calcium-rich II, (e) cluster 15 iron-rich, (f) grouped clusters 5 and 7 potassium-rich, (g) cluster 9 potassium-rich III, and (h) grouped clusters 10, 18, 19, and 20 soil dust with the temporal trend of PM<sub>10</sub> overlaid. Temporal resolution is 30 min for the single particle data and 60 min for the PM<sub>10</sub> data.
  - 2.12 Time series plots for common particle classes identified by ART-2a: cluster 1 sea salt I, cluster 2 sea salt II, cluster 8 ammonium nitrate I, and cluster 13 ammonium nitrate II. Temporal resolution is 30 min for the single particle data.
  - 2.13 Air parcel trajectory arriving at Riverside, CA 20:00 August 22, 1997. Note the air mass stagnation at the coast before landfall.
  - 2.14 Scaled size distribution plots for Riverside, CA. Plots (a) and (c) represent morning periods of elevated PM<sub>10</sub> - an average of 6:30-7:30 August 21, 7:30-8:30 August 22, and 7:30-8:30 August 23, 1997. Plots (b) and (d) represent afternoon periods of elevated ozone - an average of 14:30-15:30 August 21, 16:30-17:30 August 22, and 12:30-13:30 August 23, 1997. Each bar is pattern coded for the general chemical composition.
  - 3.1 Maps of ATOFMS sampling sites for SCOS97-NARSTO showing the air parcel trajectories for two air masses passing near Los Angeles and arriving in Azusa, CA during SCOS97-NARSTO.
  - 3.2 Positive ion digital mass spectrum of particles sampled in Los Angeles, CA on August 21, 1997.
  - 3.3 Positive ion digital mass spectrum of particles sampled in Azusa, CA on August 21, 1997. These particles are part of the same air mass as those sampled in Los Angeles (see Figure 3.2).
  - 3.4 Number of sub- $\mu\text{m}$  particles per class, identified by ART-2a (vigilance, 0.5; learning 0.05; 20 iterations, classes generated from Riverside data). Particles sampled by the ATOFMS in Los Angeles, CA on August 21, 1997.
  - 3.5 Number of sub- $\mu\text{m}$  particles per class, identified by ART-2a (vigilance, 0.5; learning 0.05; 20 iterations, classes generated from Riverside data). Particles sampled by the ATOFMS in Azusa, CA on August 21, 1997.
  - 3.6 Number of super- $\mu\text{m}$  particles per class, identified by ART-2a (vigilance, 0.5; learning 0.05; 20 iterations, classes generated from Riverside data). Particles sampled by the ATOFMS in Los Angeles, CA on August 21, 1997.
  - 3.7 Number of super- $\mu\text{m}$  particles per class, identified by ART-2a (vigilance, 0.5; learning 0.05; 20 iterations, classes generated from Riverside data). Particles sampled by the ATOFMS in Azusa, CA on August 21, 1997.
  - 3.8 Difference in the percent of sub- $\mu\text{m}$  particles matched per class, identified by ART-2a (y-axis is Azusa minus Los Angeles; classes generated from Riverside data, vigilance,

- 0.5;). Particles sampled by the ATOFMS in Los Angeles and Azusa, CA on August 21, 1997 along “trajectory 1”.
- 3.9 Difference in the percent of super-  $\mu\text{m}$  particles matched per class, identified by ART-2a (y-axis is Azusa minus Los Angeles; classes generated from Riverside data, vigilance, 0.5;). Particles sampled by the ATOFMS in Los Angeles and Azusa, CA on August 21, 1997 along “trajectory 1”.
  - 3.10 Difference in the percent of sub-  $\mu\text{m}$  particles matched per class, identified by ART-2a (y-axis is Riverside minus Azusa; classes generated from Riverside data, vigilance, 0.5;). Particles sampled by the ATOFMS in Azusa on August 21, 1997 along “trajectory 1” and Riverside, CA during August 21-23, 1997.
  - 3.11 Difference in the percent of super-  $\mu\text{m}$  particles matched per class, identified by ART-2a (y-axis is Riverside minus Azusa; classes generated from Riverside data, vigilance, 0.5;). Particles sampled by the ATOFMS in Azusa on August 21, 1997 along “trajectory 1” and Riverside, CA during August 21-23, 1997.
  - 3.12 Size distribution plots for particles matched to the common organic particle classes, identified by ART-2a (vigilance, 0.5; learning 0.05; 20 iterations, classes generated from Riverside data). Particles sampled by the ATOFMS in Azusa, CA on August 21, 1997.
  - 3.13 Positive ion “stacked” digital mass spectrum of particles sampled in Los Angeles, CA on August 21, 1997 and matched to the Riverside cluster 4 organic carbon with amines.
  - 3.14 Positive ion “stacked” digital mass spectrum of particles sampled in Azusa, CA on August 21, 1997 and matched to the Riverside cluster 4 organic carbon with amines. These particles are part of the same air mass as those sampled in Los Angeles (see Figure 3.13).
  - 3.15 Number of particles per class, identified by ART-2a (vigilance, 0.7; learning 0.05; 40 iterations, classes generated from Los Angeles dual ion data). Particles sampled by the ATOFMS in Los Angeles and Azusa, CA on August 21, 1997. Asterisks above clusters 2, 4, and 6 indicate that they are similar to “freshly emitted” motor vehicle exhaust.
  - 3.16 Normalized positive- and negative ion weight vector for a newly identified class 2 in Azusa by ART-2a (vigilance, 0.7; learning 0.05; 40 iterations, dual ion data, unlike classes generated from Los Angeles,). Particles sampled by the ATOFMS in Azusa, CA on August 21, 1997.
  - 3.17 Normalized positive- and negative ion weight vector for a newly identified class 3 in Azusa by ART-2a (vigilance, 0.7; learning 0.05; 40 iterations, dual ion data, unlike classes generated from Los Angeles,). Particles sampled by the ATOFMS in Azusa, CA on August 21, 1997.
  - 3.18 Time series plots of all particles with mass spectra sampled in Los Angeles, CA on August 21-22, 1997. The fraction of the total particles in each hour with a peak at  $m/z$  30 (area > 500) is shaded in white. Temporal resolution is 60 min. The times for the two transport trajectories are labeled.
  - 3.19 Time series plots of all particles with mass spectra sampled in Azusa, CA on August 21-22, 1997. The fraction of the total particles in each hour with a peak at  $m/z$  30 (area >

- 500) is shaded in white. Temporal resolution is 60 min. The times for the two transport trajectories are labeled.
- 3.20 Positive ion “stacked” digital mass spectrum of particles sampled in Los Angeles, CA on August 21, 1997 15:30-18:30.
  - 3.21 Positive ion “stacked” digital mass spectrum of particles sampled in Azusa, CA on August 22, 1997 8:00-11:00.
  - 3.22 Negative ion “stacked” digital mass spectrum of particles sampled in Los Angeles, CA on August 21, 1997 15:30-18:30.
  - 3.23 Negative ion “stacked” digital mass spectrum of particles sampled in Azusa, CA on August 22, 1997 8:00-11:00.
  - 4.1 Similarity plot for weight matrices from Diesel dynamometer and itself (vigilance factor 0.5).
  - 4.2 Similarity plot for weight matrices from Riverside ambient and Diesel dynamometer (both at vigilance factor 0.5).
  - 4.3 Similarity plot for weight matrices from the dual ion Diesel dynamometer and itself (vigilance factor 0.5).
  - 4.4 Similarity plot for weight matrices from the Riverside ambient and the positive ion Car dynamometer (vigilance factor 0.5).
  - 4.5 Number of particles per class, identified by ART-2a (vigilance, 0.7; classes generated from car dual ion data). Particles sampled by ATOFMS August 21-22, 1997 in Los Angeles (top) and Azusa (bottom), CA.
  - 4.6 Number of particles per class, identified by ART-2a (vigilance, 0.7; classes generated from diesel dual ion data.). Particles sampled by ATOFMS August 21-22, 1997 in Los Angeles (top) and Azusa (bottom), CA.
  - 4.7 Time series plots for particles matched to classes generated from diesel dual ion data (vigilance, 0.7;). Particles sampled by ATOFMS August 21-22, 1997 in Los Angeles (top) and Azusa (bottom), CA. Temporal resolution is 1 hour.
  - 4.8 Time series plots for particles matched to classes generated from car dual ion data (vigilance, 0.7;). Particles sampled by ATOFMS August 21-22, 1997 in Los Angeles (top) and Azusa (bottom), CA. Temporal resolution is 1 hour.
  - 4.9 Time series plot for particles matched to classes generated from car dual ion data (vigilance, 0.7;). Particles sampled by ATOFMS August 21-22, 1997 in Azusa, CA. Temporal resolution is 1 hour.
  - 5.1 Size distribution plot for the particles sampled in Mira Loma, CA September 27-29, 1997.
  - 5.2 Positive- and negative ion digital mass spectra of super-  $\mu\text{m}$  particles sampled in Mira Loma, CA during September 27-29, 1997.
  - 5.3 Positive- and negative ion digital mass spectra of sub-  $\mu\text{m}$  particles sampled in Mira Loma, CA during September 27-29, 1997.

- 5.4 Number of particles matched to ART-2a classes (vigilance, 0.5; learning 0.05; 20 iterations, classes generated from Riverside data). Particles sampled by the ATOFMS in Mira Loma, CA during September 27-29, 1997.
- 5.5 Number of sub- (left side) and super-  $\mu\text{m}$  (right side) particles matched to ART-2a classes, (vigilance, 0.5; learning 0.05; 20 iterations, classes generated from Riverside data). Particles sampled by the ATOFMS in Mira Loma, CA during September 27-29, 1997.
- 5.6 Times series plots of ATOFMS data from Mira Loma, CA. Total, super-  $\mu\text{m}$ , and particles matched to ART-2a sea salt class 1 (vigilance, 0.5; learning 0.05; 20 iterations, classes generated from Riverside data). ATOFMS data displayed with 1-hour resolution.
- 5.7 Times series plots of ATOFMS data from Mira Loma, CA. Total, sub-  $\mu\text{m}$ , and particles matched to ART-2a elemental-carbon class 16 (vigilance, 0.5; learning 0.05; 20 iterations, classes generated from Riverside data). ATOFMS data displayed with 1-hour resolution.
- 5.8 Times series plots of ATOFMS data from Mira Loma, CA. Particles matched to ART-2a sea salt class 1 and elemental-carbon class 16 (vigilance, 0.5; learning 0.05; 20 iterations, classes generated from Riverside data). ATOFMS data displayed with 1-hour resolution.
- 5.9 Times series plots of ATOFMS data from Diamond Bar, Mira Loma, and Riverside, CA. Particles selected for trajectory matched times. ATOFMS data displayed with 30 min resolution on an x-axis range 9/27/97 12:00 – 9/29/97 24:00.
- 5.10 Percent of particles per class, identified by ART-2a (positive ion, vigilance 0.7, from ATOFMS data sampled in Diamond Bar, Mira Loma, and Riverside, CA for trajectory-matched times). Particles sampled in Diamond Bar, CA September 27, 1997 11:00 – September 29, 1997 14:00.
- 5.11 Percent of particles per class, identified by ART-2a (positive ion, vigilance 0.7, from ATOFMS data sampled in Diamond Bar, Mira Loma, and Riverside, CA for trajectory-matched times). Particles sampled in Mira Loma, CA September 27, 1997 15:00 – September 29, 1997 19:00.
- 5.12 Percent of particles per class, identified by ART-2a (positive ion, vigilance 0.7, from ATOFMS data sampled in Diamond Bar, Mira Loma, and Riverside, CA for trajectory-matched times). Particles sampled in Riverside, CA September 28, 1997 00:00 – September 28, 1997 24:00.
- 5.13 Difference in the fraction of sub-  $\mu\text{m}$  particles matched per class, identified by ART-2a (y-axis is Mira Loma minus Diamond Bar; classes generated from Diamond Bar, Mira Loma, and Riverside, CA for trajectory-matched times, positive ion, vigilance 0.7). Particles sampled by the ATOFMS in Mira Loma and Diamond Bar, CA on August 27-29, 1997 (see Table 5.1 for time ranges at each site).
- 5.14 Difference in the fraction of super-  $\mu\text{m}$  particles matched per class, identified by ART-2a (y-axis is Mira Loma minus Diamond Bar; classes generated from Diamond Bar, Mira Loma, and Riverside, CA for trajectory-matched times, positive ion, vigilance 0.7). Particles sampled by the ATOFMS in Mira Loma and Diamond Bar, CA on August 27-29, 1997 (see Table 5.1 for time ranges at each site).

- 5.15 Difference in the fraction of sub-  $\mu\text{m}$  particles matched per class, identified by ART-2a (y-axis is Riverside minus Mira Loma; classes generated from Diamond Bar, Mira Loma, and Riverside, CA for trajectory-matched times, positive ion, vigilance 0.7). Particles sampled by the ATOFMS in Riverside and Mira Loma, CA on August 27-29, 1997 (see Table 5.1 for time ranges at each site).
- 5.16 Difference in the fraction of super-  $\mu\text{m}$  particles matched per class, identified by ART-2a (y-axis is Riverside minus Mira Loma; classes generated from Diamond Bar, Mira Loma, and Riverside, CA for trajectory-matched times, positive ion, vigilance 0.7). Particles sampled by the ATOFMS in Riverside and Mira Loma, CA on August 27-29, 1997 (see Table 5.1 for time ranges at each site).
- 5.17 Times series plots of ATOFMS data from Diamond Bar, CA. Particles matched to ART-2a sea salt cluster 1 and elemental-carbon class 10 (vigilance, 0.7; learning 0.05; 40 iterations, classes generated from Diamond Bar, Mira Loma, and Riverside data). ATOFMS data displayed with 30-min resolution.
- 5.18 Fraction of particles matched per class, identified by ART-2a (classes generated from Diamond Bar, Mira Loma, and Riverside, CA for trajectory-matched times, positive ion, vigilance 0.7). Particles sampled by the ATOFMS in Mira Loma and Diamond Bar, CA on August 28-29, 1997 (trajectory 3 times).
- 5.19 Difference in the fraction of particles matched per class, identified by ART-2a (classes generated from Diamond Bar, Mira Loma, and Riverside, CA for trajectory-matched times, positive ion, vigilance 0.7). Particles sampled by the ATOFMS in Mira Loma and Diamond Bar, CA on August 28-29, 1997 (trajectory 3 times).
- 5.20 Normalized weight vectors for favored of particle classes for Diamond Bar trajectory 3. Classes were identified by ART-2a, generated from Diamond Bar, Mira Loma, and Riverside, CA for trajectory-matched times, positive ion, vigilance 0.7.
- 5.21 Normalized weight vectors for favored of particle classes for Mira Loma trajectory 3. Classes were identified by ART-2a, generated from Diamond Bar, Mira Loma, and Riverside, CA for trajectory-matched times, positive ion, vigilance 0.7.
- 5.22 Normalized weight vectors for favored of particle classes for Riverside trajectory 3. Classes were identified by ART-2a, generated from Diamond Bar, Mira Loma, and Riverside, CA for trajectory-matched times, positive ion, vigilance 0.7.
- 6.1 Number of particles per class, identified by ART-2a generated from August 21-23 in Riverside. Particles sampled in Riverside, CA August 19 - September 27, 1997.
- 6.2 Number of particles per class, identified by ART-2a generated from August 21-23 in Riverside. Particles sampled in Riverside, CA August 19 - September 27, 1997.
- 6.3 Size distribution plots for particles sampled in Riverside, CA August 19 - September 27, 1997. Size resolution is 0.1  $\mu\text{m}$ ; each line represents data from a 12-hour period.
- 6.4 Size distribution plots for particles sampled in Riverside, CA August 21-23, 1997. Size resolution is 0.1  $\mu\text{m}$ ; each line represents data from a 12-hour period. No corrections have been made for offline time (shapes may be compared but intensity should not).

- 6.5 Time series plot for particles matched to cluster 8 – organic carbon with ammonium nitrate I. Temporal resolution is 3 hours for the single particle data.
- 6.6 Size distribution plot for the particles sampled in Riverside, CA September 17, 1997.
- 6.7 Number of particles matched to ART-2a classes (vigilance, 0.5; learning 0.05; 20 iterations, classes generated from Riverside data). Particles sampled by the ATOFMS in Riverside, CA during September 17, 1997.
- 6.8 Time series plot for particles matched to cluster 13 – organic carbon with ammonium nitrate II. Temporal resolution is 3 hours for the single particle data.
- 6.9 Time series plots for particles matched to organic carbon with ammonium nitrate clusters 8 and 13. Temporal resolution is 3 hours for the single particle data. The lower plot has a “zoomed-in” y-axis.
- 6.10 Time of day correlation plot for particles matched to organic carbon with ammonium nitrate cluster 8. Temporal resolution is 30 min for the single particle data.
- 6.11 Time of day correlation plot for particles matched to organic carbon with ammonium nitrate cluster 13. Temporal resolution is 30 min for the single particle data.
- 6.12 Time series plot for particles matched to sea salt with nitrate cluster 2 and ammonium nitrate organic carbon 8. Temporal resolution is 3 hours for the single particle data. The values for cluster 2 were multiplied by a factor of 2, the full height of the peaks for August 23 and September 17, 1997 extends beyond the y-axis limit of 3.4 %.
- 6.13 Time of day correlation plot for particles matched to sea salt with nitrate cluster 2. Temporal resolution is 30 min for the single particle data.
- 6.14 Time series plot for particles matched to calcium-rich dust cluster 6. Temporal resolution is 3 hours for the single particle data.
- 6.15 Time of day correlation plot for particles matched to calcium-rich dust cluster 6. Temporal resolution is 30 min for the single particle data.
- 6.16 Time series plot for particles matched to calcium-rich diesel exhaust cluster 2. Temporal resolution is 3 hours for the single particle data.
- 6.17 Time series plot for particles matched to elemental carbon with calcium diesel exhaust cluster 3. Temporal resolution is 3 hours for the single particle data.
- 6.18 Time of day correlation plot for particles matched to diesel cluster 2. Temporal resolution is 30 min for the single particle data.
- 6.19 Time of day correlation plot for particles matched to diesel cluster 3. Temporal resolution is 30 min for the single particle data.
- 6.20 Time series plot for particles matched to car cluster 2. Temporal resolution is 3 hours for the single particle data.
- 6.21 Time of day correlation plot for particles matched to car cluster 2. Temporal resolution is 30 min for the single particle data.
- 7.1 Continuous fine aerosol mass concentration as determined from the scaled ATOFMS data at Riverside during V1. Scaled ATOFMS data are shown as a solid line with shading

indicating the 95% confidence intervals; impactor data are shown as heavy horizontal bars of 4-hour duration with error bars indicating 2 standard deviations.

- 7.2 Continuous fine aerosol mass concentration as determined from the scaled ATOFMS data at Riverside during V2. Scaled ATOFMS data are shown as a solid line with shading indicating the 95% confidence intervals; impactor data are shown as heavy horizontal bars of 4-hour duration with error bars indicating 2 standard deviations.
- 7.3 Continuous fine aerosol mass concentration as determined from the scaled ATOFMS data at Riverside during N3. Scaled ATOFMS data are shown as a solid line with shading indicating the 95% confidence intervals; impactor data are shown as heavy horizontal bars of 4-hour duration with error bars indicating 2 standard deviations.
- 7.4 Pooled aerosol mass concentration data, scaled ATOFMS data versus impactor.
- 7.5 Comparison of the ATOFMS ammonium “score” (quantity of ions that would have been detected by the ATOFMS instrument if it had sized and hit all particles drawn from the atmosphere) and corresponding impactor measurements for the same time and size interval.
- 7.6 Comparison of the ATOFMS nitrate “score” (quantity of ions that would have been detected by the ATOFMS instrument if it had sized and hit all particles drawn from the atmosphere) and corresponding impactor measurements for the same time and size interval.

## List of Tables

---

- 1.1 List of ATOFMS sampling sites during SCOS97-NARSTO.
- 1.2 List of Intensive Operating Periods (IOPs) during SCOS97-NARSTO.
- 2.1 Summary of particle classes identified by ART-2a.
- 3.1 Summary of particle classes identified by ART-2a of dual ion mass spectra from Los Angeles (dual ion, vigilance factor = 0.7).
- 4.1 Summary of particle classes identified by ART-2a of positive ion mass spectra from the diesel vehicle dynamometer experiment (vigilance factor = 0.5).
- 4.2 Summary of particle classes identified by ART-2a of dual ion mass spectra from the diesel vehicle dynamometer experiment (vigilance factor = 0.5).
- 4.5 Summary of particle classes identified by ART-2a of positive ion mass spectra from the car vehicle dynamometer experiment (vigilance factor = 0.5).
- 4.6 Summary of particle classes identified by ART-2a of dual ion mass spectra from the car vehicle dynamometer experiment (vigilance factor = 0.5).
- 4.7 Summary of similarity between particle classes identified by ART-2a for positive ion mass spectra from the car vehicle dynamometer experiments and the ambient experiment in Riverside (vigilance factor = 0.5).
- 4.8 Summary of similar classes identified by ART-2a for positive ion mass spectra from the car vehicle dynamometer experiments and the ambient experiment in Riverside (vigilance factor = 0.5).
- 4.9 Summary of similarity between particle classes identified by ART-2a for dual ion mass spectra from the vehicle dynamometer experiments and the ambient data (vigilance factor = 0.7).
- 5.1 List of ATOFMS selected sampling times for each site.
- 5.2 Summary of particle classes identified by ART-2a of positive ion mass spectra from Diamond Bar-Mira-Riverside (vigilance factor = 0.7).
- 5.3 List of the characteristic particle classes from trajectory 3 sampling times for each site.
- 7.1 Parameter values fit to the scaling function  $\Phi = \alpha D_a^\beta$
- 7.2 Correlation coefficients squared ( $R^2$ ) for residual aerosol mass concentrations and aerosol concentrations of individual analytes.

## Abstract

---

Recently developed transportable aerosol time-of-flight mass spectrometry (ATOFMS) instruments and a lab-based ATOFMS instrument were used for the first long-term continuous monitoring study of the aerodynamic size and chemical composition of individual aerosol particles. This study was part of the 1997 Southern California Ozone Study-North American Research Strategy for Tropospheric Ozone (SCOS97-NARSTO) Aerosol Program. The spatial and temporal variability of aerosol particles were studied, examining the effects of transport from regions with “fresh” emissions (i.e. Los Angeles, CA) to areas of increasing pollution levels (i.e. Riverside, CA). A variety of strategies were developed to provide a picture of the particle sources and atmospheric processes occurring for particles in different regions. Procedures were developed to scale the ATOFMS data into atmospherically representative total, nitrate, and ammonium mass concentrations. Once calibrated, the ATOFMS data were plotted over time to study how particles vary over time in southern California. The instruments developed as part of this project will continue to be used in studies throughout California to provide a more complete understanding of the sources of particles as well as their spatial and temporal variability due to atmospheric transformations.

# Executive Summary

---

## ***Background***

Aerosols are defined as any solid or liquid suspended in a gas. Atmospheric aerosols have been shown to be important in many ways, ranging from causing premature death to affecting regional and global climate. Our understanding of the particle component of atmospheric aerosols is relatively limited compared to that for gas phase species. Conventional aerosol chemical analysis methods rely on filter-based sampling techniques which require sampling periods of 4-24 hours to obtain enough sample for subsequent off-line analysis. As a result, information on the temporal and spatial variability of particle composition is extremely limited (Singh 2002). Furthermore, information on the sources of particles is lacking due to the fact that most traditional bulk chemical analysis techniques average the chemical information obtained over long time scales and broad size ranges. From a health effects viewpoint, it is important to understand particle chemical variability on shorter time scales than currently available through traditional aerosol sampling and analysis methods.

## ***Objectives of research***

Three ATOFMS instruments were used in the 1997 Southern California Ozone Study-North American Research Strategy for Tropospheric Ozone (SCOS97-NARSTO) aerosol study. A major objective of the research performed involved obtaining real-time data on aerosol size and composition that can be compared with advanced aerosol models to better understand the sources and processing of particles in the environment (Kleeman 1997). Using newly developed single particle mass spectrometers such as ATOFMS, a more refined picture of particle variations can be obtained using quantitatively scaled data (Allen 2000) for mass and chemical composition (Ferguson 2001; Bhave 2002). The goal of the studies conducted in this project is to obtain a better understanding of particles sources (Bhave 2001; Song 2001) and transformations in the atmosphere in southern California.

Ideally, if particle sources can be separated by choosing the proper size cut, this would provide a more direct method for regulating particles of concern. At some locations sea salt and dust can make at times substantial contributions to PM<sub>2.5</sub>. An additional cut at 1 μm would isolate particles formed by combustion processes. Using aerosol time-of-flight mass spectrometry (ATOFMS), the goal of these studies is to determine whether unique chemical signatures at the individual particle level can be used to identify particles from specific sources in California. Furthermore, the associations of particles with nitrate, sulfate, ammonium, and carbon yield insights into secondary processes that occur on particles as they are transported over long distances. Size and composition information is obtained on short time scales and thus variations in particle size and composition are obtained with high temporal resolution. One of our primary goals is to use real-time aerosol analysis methods to elucidate the chemical associations (i.e. mixing state) in particles as functions of size and time to assist regulatory agencies in establishing proper control strategies.

## ***Methods***

The aerodynamic size and chemical composition of individual aerosol particles were analyzed continuously using aerosol ATOFMS over nearly 3 months at 5 southern California sites.

## ***Results***

Twenty publications have directly resulted from this research. Unique insights into particle composition at the single particle level have been gained. Specifically, the temporal and spatial

evolution of particle composition has been studied as particles moved across two major transport paths through the southern California air basin: Los Angeles (LA) to Azusa, and Diamond Bar to Mira Loma to Riverside. The LA/Azusa pairing showed primarily fresh vehicle emission particles identified at the single particle level by comparison with source characterization data. Azusa was also influenced by a local quarry. The Diamond Bar/Mira Loma/Riverside trajectory study showed the effects of agricultural emissions (i.e. ammonia from cows) on particles as they moved from a site upwind of the source of interest (i.e. Diamond Bar) and moved through the source region (Mira Loma) and finally into Riverside. In Riverside, the area with the highest levels of particle pollution, the complexity and major types of particles were identified. These particles were investigated over a long time period (40 days) to examine how particle composition changes over time in a specific region. Since this was the first long term study, as part of this project, new data analysis tools were developed to assist in processing these massive datasets (i.e. millions of single particle mass spectra) to allow conversion into a format that can be used for straightforward comparison and calibration with other gas and particle phase measurements. Particles can be grouped by type from specific sources which can be used for source apportionment of ambient particles (e.g. gas, diesel, biomass, meat cooking). Multivariate calibration procedures were developed that allow 44 chemical species to be quantified simultaneously. Work has also continued on optimizing the transportable instruments to detect smaller particles ( $<100$  nm) more efficiently. The newest inlet has increased our detection efficiency by 5 orders of magnitude.

### ***Conclusions***

This represented the first long-term study with transportable ATOFMS instruments, examining the temporal and spatial variability of the size and chemical composition of individual particles. Key insights into particle evolution were gained while developing new data analysis procedures to examine the massive single particle datasets. Procedures were established using data from co-located impactors that allow ATOFMS data to be converted to atmospherically relevant mass concentrations. Using the procedures developed as part of this project, for the first time, single particle mass spectral data were calibrated for ammonium and nitrate mass concentrations. Strong correlations were shown between scaled ATOFMS data and the off-line mass measurements, showing promise for these scaling procedures. In addition, based on the findings of this study, more robust ATOFMS instruments have been developed which will allow for longer term stability of the single particle data both over the course of sustained studies as well as from one study to another. In addition, a new inlet for more accurate source apportionment of aerosol particles in California has been added and tested. This new ATOFMS inlet improves aerosol detection by 5 orders of magnitude at a particle diameter of 100 nm. The findings of this study lay the groundwork for future ATOFMS applications facilitating better control aimed at particles from specific sources.

### ***Recommendations for further research***

Now that the ATOFMS instruments are fully developed, future research will involve using ATOFMS at multiple locations in California in an effort to develop a better understanding of the spatial and temporal variability of particle composition due to local sources and transformations. In an effort to develop ATOFMS into a powerful source apportionment tool, more complete and representative ATOFMS source signatures of particles from other sources as well as diesel and gasoline emissions under a variety of operating conditions will be measured. These signatures can be used to fully characterize PM in California to allow proper control strategies to be developed and improve our understanding of how particles affect human health.

# Body of Report

---

## Chapter 1 Introduction

### 1.1 Background on southern California particles

Human health, mortality, and global climate change issues regarding ambient particles are well documented (Charlson 1987; Dockery 1993; Vedal 1997; Pope 2000; Dockery 2001; Penner 2001). The Los Angeles area is notorious for generating and accumulating high levels of airborne pollutants due to the combined effects of gas and particle phase emissions primarily from vehicles along with intense sunlight, mountain-surrounded geography, and atmospheric conditions, including light winds and the common occurrence of an inversion layer (Lawson 1990; Dolislager 1999). To further our understanding of aerosols in the southern California region, intensive atmospheric measurements of particle and gas phase species were made during the Southern California Ozone Study-North American Research Strategy for Tropospheric Ozone (SCOS97-NARSTO) field campaign that took place in southern California during the summer and fall of 1997. The Southern California Air Quality Study (SCAQS), conducted 10 years prior to this study, was the only other field study conducted in southern California of this magnitude (Lawson 1990). Many of the findings from SCOS97-NARSTO are consistent with those from SCAQS (Chow 1994; Gao 1994; Turpin 1995; Eldering 1996), although new results emerged due in part to new technology developments for aerosol analysis over the past decade (McMurry 2000). During SCAQS, using mainly bulk analysis techniques, the most abundant species and the largest components of  $PM_{2.5}$  were identified as nitrate, sulfate, ammonium, organic carbon, and elemental carbon (Chow 1994). In contrast, species such as sodium, aluminum, silicon, calcium, and iron were abundant in the  $PM_{10}$  fraction. However, the combinations of chemical species present on individual particles could not be identified during SCAQS and previous studies. Information on the chemical associations as a function of particle size is vital to understanding the sources of the particles, subsequent chemistry the particles undergo in the atmosphere, as well as the health effects of particles (Thomas 2002).

This chapter focuses on real-time single particle mass spectrometry measurements made with an aerosol time-of-flight mass spectrometer (ATOFMS) in Riverside, an area situated on the eastern edge of the Los Angeles air basin and characterized by extended periods of high smog levels and poor air quality. ATOFMS was one of the first real-time single particle mass spectrometry (SPMS) techniques to be used in field campaigns. A number of recent reviews describe the various SPMS instruments (Suess 1999; Johnston 2000). Murphy et al. have performed extensive ambient sampling using PALMS in other areas of the U.S. and world (Murphy 1998; Murphy 2000), however until recently, the majority of single particle measurements have focused on simplistic, laboratory generated particles (Neubauer 1998; Kane 2001; Phares 2001; Kane 2002). Subtle yet fundamental differences in each of the instruments general operating principles leads to differences in the information they provide, particularly on size-resolved chemistry (Middlebrook 2003). The ability to size particles in PALMS is limited by the light scattering method used for particle detection (Lee 2002). Other SPMS instruments select a specific particle size and must step through multiple discrete sizes, limiting the size resolution and increasing the time required to fully interrogate a statistically representative

number of atmospheric particles (Mallina 2000; Held 2002). SPMS instruments have the potential to provide unique insights into atmospheric aerosols, however currently a bottleneck associated with processing the extensive ambient datasets exists. A number of efforts are underway to develop routine procedures which can be used to extract information from the data in formats that allow for rapid comparison with other particle, gas phase, and meteorological measurements (Hinz 1999; Phares 2001; Bhave 2002; Held 2002; Tan 2002). This chapter focuses on some of the methodologies used in our laboratory as well as the unique insights single particle data can provide once the data are reduced to the proper format (Pastor 2003).

Three aerosol time-of-flight mass spectrometers analyzed particulate matter in different locations in the Los Angeles Basin. From June until October 1997, the lab-based ATOFMS instrument sampled in Riverside. In addition to the ATOFMS instruments, electrical aerosol analyzers and laser optical particle counters measured particle size distributions. During intensive sampling periods, fine particle ( $<1.9 \mu\text{m}$ ) and  $\text{PM}_{10}$  filter samplers were used to obtain bulk chemical composition data. Particles in several size ranges were measured using a pair of micro-orifice uniform deposit (MOUDI) impactors at each site for selected times during the intensive sampling periods in order to scale the ATOFMS data using a procedure described previously (Allen 2000).

This chapter describes the size-resolved composition observed for particles with aerodynamic diameters between 0.2 and 1.6  $\mu\text{m}$  sampled in Riverside. The ATOFMS provides unique information on the combinations of chemical species present in individual particles as a function of particle size, such as the couplings between sulfates and nitrates with specific particle types in the different size modes. In general, the strength of single particle mass spectrometers lies in the ability to obtain individual particle fingerprints for performing source identification and apportionment, as well as monitoring secondary transformations on particles. The ultimate goal is to use the chemical associations observed in single particle data for model comparisons (Kleeman 1997; Kleeman 2001; Bhave 2002), as well as to provide input into atmospheric aerosol models (Pandis 1992; Jacobson 1999).

The individual particle size and chemical data in Riverside were acquired with high temporal resolution to allow direct (hour by hour) comparisons to be made between the particle types observed with gas phase (i.e. ozone), meteorology, and visibility data. Data collected over a 3-day period between August 21 and 23, 1997 are discussed, comparing and contrasting the aerosol size and composition distributions observed during periods with elevated ozone and  $\text{PM}_{10}$  levels.

## **Materials and Methods**

### **1.2 SCOS-NARSTO Aerosol Program**

During the summer and fall of 1997, several agencies co-sponsored the Southern California Ozone Study-North American Research Strategy for Tropospheric Ozone (SCOS97-NARSTO) field campaign which took place in southern California (Motallebi 1998; Wood 1998; Collins 2000; Liu 2000; Pastor 2000; Vuilleumier 2001; Klouda 2002). Air quality was investigated at multiple locations with a variety of techniques. The four-month investigation, running from mid-June through mid-October 1997, measured ozone, ozone precursors (such as hydrocarbons and nitrogen oxides), and meteorology. Both ground-based and aircraft measurements were

made. The results support ongoing ozone modeling and analysis efforts with the goal of obtaining more precise and effective measures to reduce ozone in southern California.

The aerosol program within the larger SCOS97-NARSTO study focused on the particulate air quality in southern California. The human health, human mortality, and global climate change issues regarding ambient particles are well documented (Dockery 1993; Pope III 1995; Vedal 1997; Penner 1998; Pope 2000; Penner 2001). The goals of the SCOS97-NARSTO study came from both regulatory and scientific perspectives. In general, the goals included examining the relationships between motor vehicle emissions and ambient aerosols, secondary aerosol processes, the contributions of various sources to both primary and secondary particle burdens in the atmosphere, and the movement and evolution of aerosol-laden air masses across the region. As part of SCOS97-NARSTO, three ATOFMS instruments were used to characterize individual particle size and composition in real-time, examining the spatial and temporal variations of the southern California aerosol.

ATOFMS data reveal the particle types present with high time resolution, in contrast to the time-averaged, bulk chemical properties of the particles sampled using conventional filter-based methods. This study allowed for the characterization of aerosols in near-coastal, mid-region, and interior locations in southern California by ATOFMS, including for the first time the use of transportable instruments to obtain positive- and negative ion mass spectra from the same particle. The data from this study allowed for the comparison of the ATOFMS data with other measurements (including ozone and visibility), the observation of particle transformation between sampling sites, the determination of long term trends in single particle composition, the continued development of detection efficiency calibration functions for the ATOFMS instruments, and the demonstration and testing of new data analysis approaches for ATOFMS quantification and source apportionment.

The laboratory-based ATOFMS instrument sampled in Riverside throughout the study. Two transportable instruments sampled at several locations including Central Los Angeles, Azusa, Diamond Bar, Mira Loma, Riverside, and Mt Wilson (see Figure 1.1 and Table 1.1, note: Mt Wilson is located ten miles northwest of Azusa).

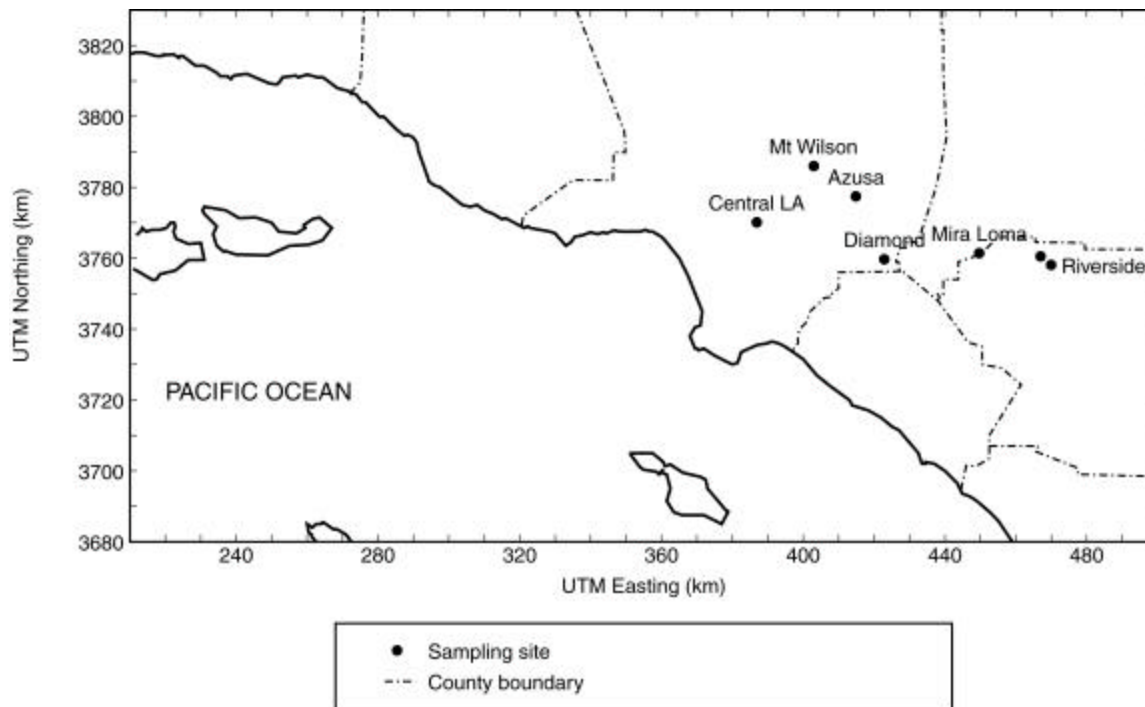


**Figure 1.1: Map of ATOFMS sampling sites during SCOS97-NARSTO.**

**Table 1.1: List of ATOFMS sampling sites during SCOS97-NARSTO.**

| Date                   | Sampling Location         | ATOFMS instrument   |
|------------------------|---------------------------|---------------------|
| mid-June – mid-October | Riverside Pierce Hall UCR | lab-based (BST)     |
| late June – early July | Riverside CE-CERT         | transportable (JKE) |
| late June – early July | Mt. Wilson                | transportable (ELD) |
| August                 | Central Los Angeles       | transportable (JKE) |
| August                 | Azusa                     | transportable (ELD) |
| September              | Diamond Bar               | transportable (JKE) |
| September              | Mira Loma                 | transportable (ELD) |

## Results

### 1.2.1 Riverside Aerosol Characterization

As noted in Chapter 2, although the summer of 1997 was relatively unpolluted compared to previous years, Riverside, CA still registered elevated ozone and particulate matter (PM<sub>10</sub>) levels. Hourly-averaged afternoon ozone levels of almost 150 parts per billion were observed. Aerosol size and composition distributions were examined during periods of elevated ozone and particulate matter (PM<sub>10</sub>) levels as well as times with decreased visibility.

For the ATOFMS data analysis discussed in Chapter 2, the application of a neural network allows for particle classification by a mathematical algorithm; the specific adaptive resonance algorithm used is known as ART-2a. In contrast to rules-based searching, where the analyst must define the particle types, the neural network groups particles with similar composition (i.e. mass spectral intensities) without any prior biases or expectations. All of the peaks in the mass spectrum contribute to the particle classification (based on relative intensity) as opposed to just a few peaks, as used for rules-based searching. The particle types observed in Riverside were characterized by distinct size-composition relationships. Air parcel trajectories showing the air mass history were used to relate the particle types with specific trajectories or sources. ATOFMS, using the measured single particle associations, clearly show an overall particle size and composition change between the mornings and the afternoon periods on August 21-23 (Chapter 2).

### 1.2.2 Los Angeles-Azusa Aerosol Evolution

Chapter 3 discusses the evolution of particles moving across the region. During SCOS97, ATOFMS instruments were used to sample particles in several locations situated along common wind trajectory paths in the Los Angeles region. This strategic selection of sampling locations allowed for the characterization of particle transformations occurring as the air parcels moved from one site to another. Throughout the study, the lab-based ATOFMS instrument sampled in Riverside. Two transportable instruments sampled in Central Los Angeles and Azusa in August (see Table 1.1). Common wind trajectories for this region place the Azusa sampling site downwind of the central Los Angeles sampling site. Air parcel trajectories were used to identify times of site-to-site air mass transport. The central Los Angeles site is in close proximity to freeways and thus likely to capture a snapshot of single particles from fresh vehicle emissions. The central Los Angeles site is located about 15 miles from the coast. The Azusa site is located mid-region, about 35 miles from the coast and at the foot of the San Gabriel Mountains (north edge of the valley). The Riverside site is 30 miles further downwind and thus likely to show the most aged particles of all sites.

Rapid site-to-site movement across the region characterized one trajectory. In comparison to Los Angeles, the size profiles of common organic carbon classes shifted to slightly larger sizes when in Azusa, suggesting growth of the particles occurred during transport. The particles were matched to the classes generated when characterizing the particles in Riverside. A dual ion, more strict classification of the Los Angeles and Azusa data by the neural network produced “fresh-emission” classes that occurred predominately in Los Angeles and amine-rich “aged-emission” classes that appeared in Azusa. Other dust and sea salt classes were observed at both sites.

A second trajectory was characterized by the stagnation of the air mass between the Los Angeles and Azusa sampling sites. Particle enrichment of nitrate, sulfate, organics, amines, and other species were observed in the stagnating air mass. A diurnal variation of the nitrate-rich particles was observed on August 21 and 22. The composition of the air mass in Los Angeles and Azusa is displayed in the form of dual ion "stacked" digital mass spectra that illustrate these changes (Figures 3.20-3.23).

### **1.2.3 Source Characterization**

Data from a field campaign of this magnitude produce many opportunities, as well as new and unique challenges. In Chapter 4 ambient particles are compared to vehicle emission signatures obtained in a dynamometer source characterization experiment to identify individual ambient particles from Los Angeles and Azusa (sampling sites with potential motor vehicle influence). The matching of ambient particles to these source signatures provides a demonstration of the advanced source allocation tools made available by using databases and neural networks for the data analysis. This and similar developments, although time consuming to initially implement, will make the timely analysis of large, complex datasets more feasible for future studies.

The motor vehicle signatures were created from an ATOFMS dataset of tailpipe vehicle emissions obtained in a study conducted at the California Air Resources Board Haagen-Smit facility in El Monte, CA. This study was the first vehicular study conducted with ATOFMS, the fleet of vehicles was limited, and the number of overall particles sampled quite small. Therefore, the results are shown to demonstrate the potential of such an approach. Particle classes were determined for the car and diesel sources using the ART-2a neural network. The ambient classes were then compared to the source signatures. The organic carbon with amines and elemental carbon particle types were found to have significant overlap between the dynamometer source test and the SCOS97-NARSTO ambient data. The ambient datasets, including those of Azusa and Los Angeles, were searched for particles with these source "fingerprints." The ATOFMS data from the dynamometer, Azusa, and Los Angeles sites included negative ion mass spectral data. These were also considered for the source characterization. The vigilance factor, a factor in the neural network that sets the required degree of similarity between particles in a class, was adjusted and the results from the analysis at a vigilance factor of 0.7 are contrasted to the results at 0.5. Further source characterization studies continue in our laboratory. This study represents the first demonstration of combining data from ambient studies with source characterization studies with the ultimate goal being to have large enough source characterization datasets and the necessary data analysis tools to allow for ambient source apportionment at the single particle level.

### **1.2.4 Mira Loma and Nitrate-Oriented Trajectory**

Chapter 5 discusses data obtained at the Mira Loma sampling site which provided a mid-region point in an air parcel trajectory across the valley. The abundance of the particle types is considerably different than Riverside. During the late September period, September 27-29, 1997, elemental carbon was a common particle type, perhaps due to the close proximity of the freeway and the diesel truck activity at the site. Despite the nearby dairy feedlots, no particles were classified in the organic carbon with ammonium nitrate cluster observed for particles sampled in

Riverside. However, even though relatively low in intensity, the marker peaks of 18 and 30 were present in some of the particles sampled in Mira Loma. In addition, potassium-rich particles were common in the sub-  $\mu\text{m}$  mode, indicating possible biomass/biofuel burning.

### 1.2.5 Trends in the Riverside Aerosol

The final chapter of this report, Chapter 6, reports the aerosol size and composition observed using ATOFMS over 40 days in Riverside. The particle size distributions are compared. The trends of the various particle types, including source classes or “fingerprints,” are tracked, periods of elevation or absence pinpointed, and the temporal trends among classes contrasted. The results show the benefits of long term monitoring of particle chemistry. The observed trends should ultimately allow for a better understanding of aerosol sources and chemistry in the atmosphere.

## 1.3 Air Quality during the SCOS97-NARSTO Sampling Period

Within the long timeframe of the SCOS97-NARSTO study, certain days were selected as intensive operating periods (IOPs). Transport patterns and air quality episodes of interest were expected on these days. Some of the non-continuous instruments were used for sampling on/around these targeted days. Several classes of IOPs during the SCOS97-NARSTO study are listed in Table 1.2. Various IOPs had significant overlap.

Some of the IOPs are also noted in Figure 1.2, which shows the hourly ozone, and  $\text{PM}_{10}$  data for Riverside. The  $\text{PM}_{10}$  data were recorded by a tapered element microbalance (TEOM). The hourly average ozone in Riverside on August 15 – October 31, 1997 peaked at 140 ppb on August 23. The hourly  $\text{PM}_{10}$  level spiked between 125-150  $\mu\text{g m}^{-3}$  on several days.

**Table 1.2: List of Intensive Operating Periods (IOPs) during SCOS97-NARSTO.**

| Prather/Cass IOPs | Ozone IOPs      | Aerosol (aircraft) | Tracer      |
|-------------------|-----------------|--------------------|-------------|
| ---               | July 14         | ---                | ---         |
| ---               | August 4-7      | ---                | ---         |
| August 21-22      | August 22-23    | August 22          | August 23   |
| August 27-28      | ---             |                    |             |
| September 4-5     | September 3-6   | September 4-5      | September 4 |
| September 27      | September 27-29 | September 28-29    | ---         |
| ---               | October 3-4     | ---                | October 4   |

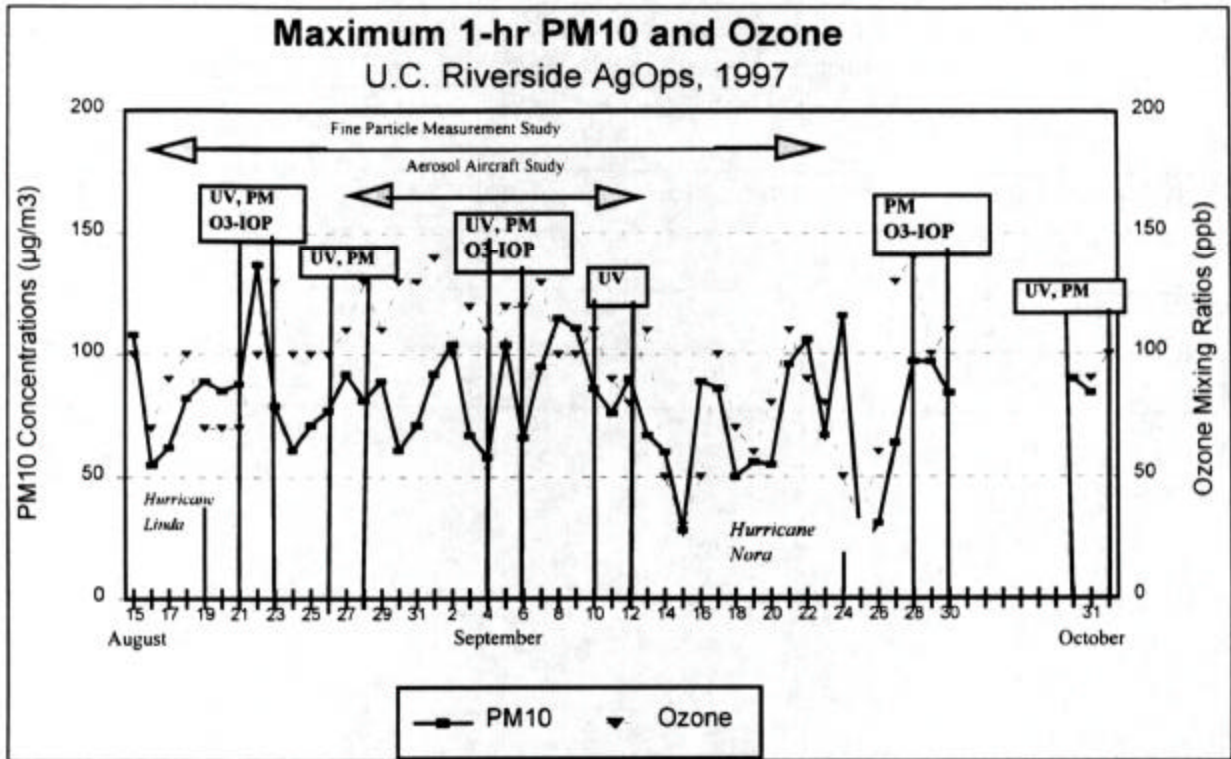


Figure 1.2: Daily maximum one-hour TEOM PM<sub>10</sub> and ozone concentrations during SCOS97-NARSTO in Riverside, CA. Adapted from Fujita et al, 1999 (Volume III).

## Chapter 2

# Riverside Aerosol Characterization

### 2.1 Overview

This chapter focuses on real-time single particle mass spectrometry measurements made with an aerosol time-of-flight mass spectrometer (ATOFMS) in Riverside, an area situated on the eastern edge of the Los Angeles air basin and characterized by extended periods of high smog levels and poor air quality. ATOFMS was one of the first real-time single particle mass spectrometry (SPMS) techniques to be used in field campaigns. A number of recent reviews describe the various SPMS instruments (Suess 1999; Johnston 2000). Murphy et al. have performed extensive ambient sampling using PALMS in other areas (Murphy 1998; Murphy 2000), however until recently, the majority of single particle measurements have focused on simplistic, laboratory generated particles (Neubauer 1998; Kane 2001; Phares 2001; Kane 2002). Subtle yet fundamental differences in each of the instruments general operating principles lead to differences in the information they provide, particularly on size-resolved chemistry (Middlebrook 2003). The ability to size particles in PALMS is limited by the light scattering method used for particle detection (Lee 2002). Other SPMS instruments select a specific particle size and must step through multiple discrete sizes, limiting the size resolution and increasing the time required to fully interrogate a statistically representative number of atmospheric particles (Mallina 2000; Held 2002). SPMS instruments have the potential to provide unique insights into atmospheric aerosols, however currently a bottleneck associated with processing the extensive ambient data sets exists. A number of efforts are underway to develop routine procedures which can be used to extract information from the data in formats that allow for rapid comparison with other particle, gas phase, and meteorological measurements (Hinz 1999; Phares 2001; Bhave 2002; Held 2002; Tan 2002). This report focuses on some of the methodologies used in our laboratory as well as the unique insights single particle data can provide once the data are reduced to the proper format.

In this chapter, the size and chemical composition of individual ambient particles in Riverside, CA during the summer of 1997 are described. Data collected using co-located MOUDI impactors are used to scale the ATOFMS number counts, providing a unique picture of the particle population which complements information obtained using traditional sizing and composition analysis techniques in this and previous studies. Changes in single particle composition are observed over time, and compared and contrasted with observed changes in visibility, ozone, and PM<sub>10</sub> concentrations. Details are provided on changes in the particle size and composition observed during three morning periods with low ozone and elevated PM<sub>10</sub> versus three afternoon periods with both elevated ozone and PM<sub>10</sub> levels between August 21-23, 1997. The ATOFMS size profiles show afternoon periods dominated by sub- $\mu\text{m}$  particles composed of organic carbon coupled with ammonium nitrate, and morning periods with relatively high levels of super- $\mu\text{m}$  dust particles. The observed changes in particle size and composition are consistent with differences in air mass trajectories arriving at Riverside during the morning and afternoon time periods.

Intensive air sampling measurements were made during the time period August 21-23, 1997 in Riverside, CA due to elevated ozone and particulate matter levels (hourly PM<sub>10</sub> are discussed, hourly PM<sub>2.5</sub> data were not available). Data collected during this 3-day period are discussed to compare and contrast the aerosol size and composition distributions observed during this period. The information obtained using aerosol time-of-flight mass spectrometry (ATOFMS) provides a unique picture of the particle population, complementing information obtained with traditional sizing and composition analysis techniques. Rapid changes in single particle composition were observed, and compared and contrasted with observed changes in visibility, ozone levels, and particulate matter levels. Air parcel trajectories showing the air mass history can be used to relate the particle types with specific trajectories or sources. In addition to the ATOFMS instruments, an electrical aerosol analyzer and a laser optical particle counter measured particle size distributions. During intensive sampling periods, including August 21-22, fine particle and PM<sub>10</sub> filter samplers were used to obtain bulk chemical composition data. The chemical compositions of particles in several size ranges were measured using a pair of micro-orifice impactors (MOUDI) at each site for selected times during the intensive sampling periods (Allen 2000).

Particles between 0.2 and 3.5  $\mu\text{m}$  in aerodynamic diameter were sampled and analyzed by the laboratory-based ATOFMS instrument in Riverside. Positive ion time-of-flight mass spectra were obtained for approximately 30% of the sized particles. The analysis of the positive ion ATOFMS data generates a description of the particle composition with high time and size resolution. Temporal plots are typically obtained with 10-60 minute resolution at ambient particle concentrations (Liu 2000; Guazzotti 2001; Guazzotti 2001), and changes in particle size of approximately 25-40 nanometers are detectable (Noble 1996). An adaptive resonance algorithm was used to classify particles (Song 1999; Phares 2001). As described herein, the analysis of ATOFMS data reveal particle sizes and compositions that correlate with elevated ozone and PM<sub>10</sub> levels, as well as air mass trajectories that correlate with specific particle types.

Detection efficiency scaling factors were derived and used to compensate for the characteristic size biases of the ATOFMS instruments. Scaled number concentrations are presented to contrast the size and composition observed in the morning periods, with low ozone and elevated PM<sub>10</sub>, and afternoon periods, with elevated ozone and PM<sub>10</sub>, as well as decreased visibility. No direct correlation exists between PM<sub>10</sub> and visibility during this sampling period in Riverside. In fact, the visibility was not significantly reduced when PM<sub>10</sub> was at the highest level in the 3-day period. Micro-orifice impactors were only run for two four-hour afternoon periods in Riverside during these three days because of analysis cost considerations. The Cass research group collected fine (<1.9  $\mu\text{m}$ ) and coarse (<10  $\mu\text{m}$ ) particle filter samples on a 5-sample per day schedule. These conventional bulk mass distribution measurements lacked the size and temporal resolution necessary to explain the changes in air quality and visibility. However, ATOFMS, using the measured single particle associations, clearly shows an overall particle size and composition change between the mornings and afternoon periods. In this chapter, we describe the particle types observed in Riverside, illustrating the distinct size-composition relationships observed.

## 2.2 Experimental methods

The general technique, aerosol time-of-flight mass spectrometry (ATOFMS), is described along with the operating principles of the ATOFMS instruments in a number of previous publications (Prather 1994; Noble 1996; Gard 1997). ATOFMS instruments perform real-time

detection and characterization of single particles from polydisperse samples, supplying information on aerodynamic size and composition. The lab-based ATOFMS instrument sampled air from a second floor window of the Chemistry building on the University of California – Riverside campus continuously from June 29-September 30, 1997.

ATOFMS instruments pull air through a reduced pressure sample inlet region. A converging nozzle followed by a region of differential pumping with skimmers creates a narrow particle beam. Each particle is accelerated to a size-dependent terminal velocity. Particles in the collimated beam scatter light as they cross continuous-wave diode laser beams. The velocity of each particle is determined by the transit time between two continuous-wave laser beams a known distance apart. The aerodynamic diameter is calculated from a calibration curve relating the velocity of the particle to an aerodynamic diameter. The velocity of the particles is used to time the firing of a pulsed laser – a frequency quadrupled Nd:YAG (266 nm, Continuum) – to desorb/ionize chemical species from the particle. The ions generated from the ablation process are analyzed by time-of-flight mass spectrometry. The lab-based instrument used for this study in Riverside is capable of detecting either positive or negative ion mass spectra; transportable ATOFMS instruments collect both positive and negative ion mass spectra simultaneously. During this study in Riverside, about thirty minutes of every three hours were dedicated to negative ion data collection. Positive and negative ion mass spectra provide complementary information on the chemical species present in the particles. Since the data are not directly comparable, only the periods where positive ion spectra were acquired are discussed in this chapter. A break appears in the temporal plots for each thirty-minute period when negative ion mass spectra were being acquired.

The single particle ATOFMS data are calibrated for size using a calibration curve that is generated by measuring the velocity of ammonium sulfate  $(\text{NH}_4)_2(\text{SO}_4)$  particles generated with a vibrating orifice aerosol generator (VOAG; TSI, Inc.) and polystyrene latex spheres (PSL) of known aerodynamic diameter. The size calibration was performed in the range  $0.2 \mu\text{m} < D_a < 1.8 \mu\text{m}$  and extrapolated to  $3.5 \mu\text{m}$ . The mass spectra are calibrated using custom written software. Peak lists are generated for each mass spectrum collected. A peak threshold of 10 units above baseline and an area threshold of 12 units on a 256-unit scale were used in creating the peak lists.

The detection efficiency calibration functions for the Southern California Ozone Study were derived in an analogous manner to those developed by Allen and co-workers for a study that took place in southern California in 1996 (Allen 2000). The particle detection efficiency is a function of particle aerodynamic diameter ( $D_a$ ). For the lab-based instrument, the calibration equation used for this study is  $N = 1500(D_a)^{-4.2}$ . Note this represents the average value calculated for the entire study obtained using all calibration points. Further details on how this equation changed over the course of the study are given in Bhave et al. (Bhave 2002). Applying a single calibration equation to the entire study simplified the overall calibration procedure, however in future studies, different calibrations corresponding to specific periods of the study will be used. For a given volume of air, the number of particles present in the ambient air sample,  $N$ , may be calculated using the size of each particle observed by ATOFMS. The application of the scaling factors to a size distribution has a larger effect on smaller particles, due to their smaller detection efficiency. The ATOFMS inlet used during the present study focused a narrow size range of particles very efficiently, leading to enhanced particle detection in the 1.6-1.8  $\mu\text{m}$  size range. Because this size interval is much narrower than the corresponding size range of MOUDI measurements used to calibrate these data (1.0-1.8  $\mu\text{m}$ ), the MOUDI calibration could not

account for the ATOFMS focusing effect, so the ATOFMS data above 1.6  $\mu\text{m}$  are disregarded in the present work. In future studies, calibration will be attempted using aerosol instruments

The neural network scheme used for mass spectral classification is an adaptive resonance algorithm, known as ART-2a (Carpenter 1991). ART-2a identifies classes of particles based on similarities in their compositions (mass spectral intensity patterns), and has previously been applied to sets of single particle data, including ATOFMS data (Hopke 1997; Song 1999; Liu 2000; Phares 2001). Matlab (Mathworks Inc.) is the software platform used for the ART-2a analysis. A database, YAADA (“Yet Another ATOFMS Data Analyzer”; see [www.yaada.org](http://www.yaada.org)), manages and allows for the analysis of single particle ATOFMS data (Allen, Ferguson, Pastor et al., 2000). The data are imported into YAADA (Yet Another ATOFMS Data Analyzer; see [www.yaada.org](http://www.yaada.org)), an object-oriented toolbox written in the Matlab programming language (Matlab versions 5.3 and 6.0 were used for this analysis). Pentium-based PC computers running Windows are used for data processing. Each particle to be analyzed by ART-2a is converted into a normalized vector where each point represents a whole  $m/z$  unit in the mass spectrum. ART-2a groups particles that have sufficiently similar vectors. Each class or cluster of particles has an associated weight vector which describes the “quintessential” mass spectrum for that class. Clusters determined by the neural network are compared and classes with similar chemical composition, size, and temporal profiles may be combined if necessary. The set of weight vectors for each particle type is called a weight matrix. The parameters for the ART-2 analysis of the Riverside dataset were: a vigilance factor (VF) of 0.5, a learning rate of 0.05, a maximum of 20 iterations, and a range of the first 350  $m/z$  ( $m/z$ ) units of the positive ion mass spectra for creating the vectors. The vigilance factor can be changed to define how closely the particle mass spectra must resemble one another to be grouped into the same class. A VF of 0.5 is considered loose, meaning particles can have a relatively wide range of compositions and fall in the same class. For ambient measurements, this value has proven to be the most appropriate for developing a rapid and general picture of a large ambient dataset. In other chapters in this report, higher VF values are used and the results are compared. The highest VF is 1.0 and this is the value to two completely identical particles (mass spectra).

In order to facilitate the ART-2a analysis, an initial subset of particles (10,000-20,000) was analyzed to determine the major particle types. The initial analysis set contained 11,480 particles from eight 1-hour time periods starting with the following times: August 21, 1997 at 1:00, 12:00, 21:00; August 22, 1997 at 6:00, 15:00, 24:00; and August 23, 1997 at 9:00, 18:00. This initial dataset created a matrix of weight vectors, one for each class of particles. Then each particle in this three-day ATOFMS dataset was classified into these types. All particles that could not be classified by the existing types were analyzed by a second ART-2a analysis, generating additional classes in the form of a second weight matrix. Finally, the combined set of classes from both ART-2a analyses was used to classify the entire set of particles a final time. In summary, four general steps were taken to arrive at the final particle classes from the ART-2a analysis: ART-2a analysis of the initial dataset, matching the full set to those classes, ART-2a analysis of unclassified particles with the generation of additional classes, and matching the full set to the combined set of classes.

The South Coast Air Quality Management District (SCAQMD) provided the ozone and  $\text{PM}_{10}$  hourly data. Electric Power Research Institute (EPRI) provided the hourly nephelometer data. EPRI and Harvard University - School of Public Health (HSPH) provided daily  $\text{PM}_{2.5}$  mass data. These measurements were all made at the University of California Agricultural Operations Field site about a mile from the ATOFMS sampling site. Air parcel trajectory plots created by

backward integration through hourly wind fields were calculated from the wind speed and direction observations from about 30 sites in the air basin. In this study, the trajectories of air parcels arriving hourly at Riverside on August 21 - 23, 1997, were calculated using the method of Goodin et al. (Goodin 1979).

## 2.3 Results and Discussion

### 2.3.1 ART-2a Analysis of ATOFMS Data from August 21-23, 1997

The Riverside ATOFMS collected 90,585 positive ion mass spectra of individual particles during the three-day period from August 21 to 23, 1997. 41 classes (or clusters) remained after the initial ART-2a results were generated and truncated to include only classes containing 20 or more particles. Each particle in the full 3-day dataset was then compared to the 41 weight vectors. Particles that could not be classified into one of these 41 classes were classified by the second ART-2a analysis, generating 16 additional clusters that contained 20 or more particles. Finally, all of the particles from the three-day period were reclassified into the 57 available clusters based on their similarity to the weight vectors. These clusters were sorted and assigned numbers based on the number of spectra explained by each cluster (Figure 2.1). Of the analyzed particles, 70% were accounted for by the top 10 clusters, 86% by the first 20, 95% by the first 30, and 98% by the top 40 clusters. Less than 0.5% of the particles (488 out of 90,585) did not match any of the 57 weight vectors within the vigilance factor of 0.5.

A summary of cluster information for the 20 most populated clusters, based on unscaled ATOFMS counts, is given in Table 2.1. The weight matrices for the top clusters are shown in Appendix C. For the purpose of discussion, the most populated cluster based on detected particle counts, is referred to as cluster 1, the second most populated as cluster 2, and so on. ATOFMS instruments preferentially detect larger particles so the rank order of the types will be different for detection-efficiency scaled ATOFMS data (Allen 2000). The 12 most intense peaks are listed for each cluster. To provide an indication of the relative intensity of the peaks within each weight vector, the  $m/z$  ratios ( $m/z$ ) are presented in coded typeface. The use of boldface and/or underlining indicates the peak's normalized intensity. Peaks with a normalized intensity greater than 0.75 are listed in boldface and underlined. Peaks with a normalized intensity less than 0.75 but greater than 0.50 are underlined. Peaks with a normalized intensity less than 0.50 but greater than 0.25 are listed in bold. Finally, peaks with normalized intensities less than 0.25 are neither boldfaced nor underlined. The characteristic chemical markers in each the 20 dominant clusters are briefly assigned in the far right column of Table 2.1. The particle mass spectra detected in Riverside show markers for amines, ammonium nitrate, calcium, iron, organic carbon, elemental carbon, sea salt, and other particle types (see Appendix A for a list of  $m/z$  values with possible mass spectral peak assignments). One of the advantages of single particle techniques is this ability to identify not only the species present but also the species combinations. In the case of single particle mass spectrometry techniques, like ATOFMS, that also collect particle size information, the size range in which the species occur can be determined with high resolution. These top 20 clusters will be discussed in further detail, including their chemical composition, size, and temporal profiles 40 days of sampling. The particle types observed in Riverside show distinct size-composition relationships. The particle types present during morning peaks of high  $PM_{10}$  and low ozone are contrasted with the particle types present during afternoon periods with high ozone,  $PM_{10}$ , and  $b_{scat}$ .

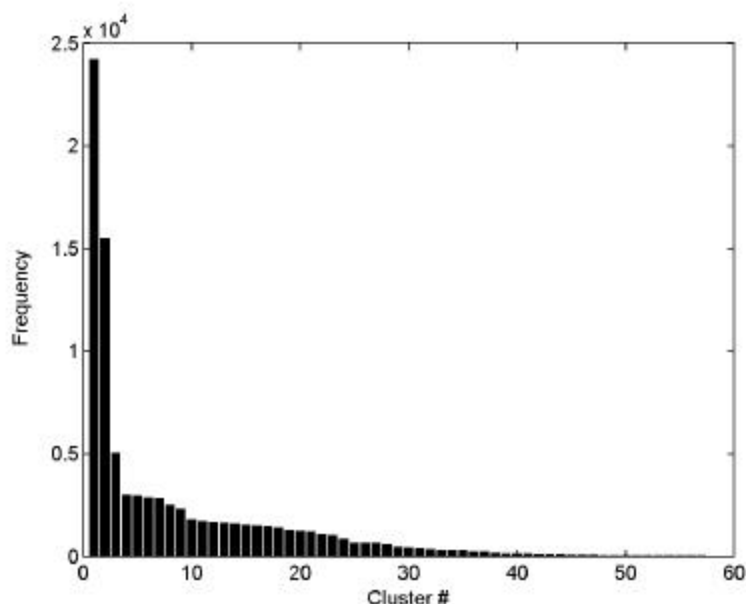


**Figure 2.1:** Number of particles per class, identified by ART-2a (vigilance, 0.5; learning 0.05; 20 iterations). Particles sampled by the lab-based ATOFMS in Riverside, CA on August 21-23, 1997.

**Table 2.1:** Summary of particle classes identified by ART-2a.

| Class | No. in Class | Top 12 Peaks (m/z)* |           |           |           |           |           |           |    |     |     |     |    | Brief Description         |
|-------|--------------|---------------------|-----------|-----------|-----------|-----------|-----------|-----------|----|-----|-----|-----|----|---------------------------|
|       |              | *Normalized Area    |           |           |           |           |           |           |    |     |     |     |    |                           |
|       |              | >0.75               | 0.5-0.75  | 0.25-0.50 | <0.25     |           |           |           |    |     |     |     |    |                           |
| 1     | 24,234       | <u>23</u>           | 39        | 24        | 40        | 63        | 41        | 46        | 36 | 62  | 108 | 25  | 30 | sea salt, nitrate         |
| 2     | 15,488       | <u>23</u>           | <u>24</u> | <b>39</b> | 40        | 25        | 63        | 41        | 26 | 62  | 108 | 165 | 46 | sea salt, nitrate         |
| 3     | 5,061        | <u>40</u>           | <u>23</u> | <b>41</b> | 24        | 57        | 39        | 56        | 59 | 42  | 44  | 25  | 26 | calcium-rich dust         |
| 4     | 3,034        | <b>27</b>           | <b>37</b> | <b>18</b> | <b>43</b> | <b>36</b> | <b>12</b> | <b>30</b> | 39 | 29  | 24  | 86  | 38 | organic carbon, amines    |
| 5     | 2,997        | <u>39</u>           | <b>40</b> | <b>41</b> | 23        | 57        | 56        | 27        | 24 | 140 | 72  | 42  | 64 | potassium-rich dust       |
| 6     | 2,891        | <u>40</u>           | <b>57</b> | <b>56</b> | 41        | 27        | 39        | 113       | 23 | 24  | 42  | 96  | 44 | calcium-rich dust         |
| 7     | 2,861        | <u>39</u>           | 23        | 41        | 56        | 24        | 1         | 40        | 27 | 43  | 18  | 42  | 36 | potassium-rich dust       |
| 8     | 2,509        | <u>30</u>           | <b>18</b> | 12        | 35        | 36        | 27        | 31        | 46 | 17  | 37  | 24  | 43 | nitrate, ammonium, carbon |

|    |       |           |           |           |           |           |    |    |    |    |    |    |    |                           |
|----|-------|-----------|-----------|-----------|-----------|-----------|----|----|----|----|----|----|----|---------------------------|
| 9  | 2,338 | <u>39</u> | <b>27</b> | <b>23</b> | 40        | 56        | 41 | 24 | 28 | 57 | 1  | 25 | 26 | potassium-rich dust       |
| 10 | 1,783 | <u>1</u>  | <b>23</b> | <b>24</b> | <b>27</b> | 39        | 16 | 25 | 26 | 40 | 38 | 28 | 22 | soil dust                 |
| 11 | 1,718 | <u>37</u> | <b>36</b> | <b>27</b> | 43        | 18        | 38 | 39 | 12 | 86 | 50 | 24 | 30 | Organic carbon, amines    |
| 12 | 1,701 | <u>18</u> | <b>37</b> | <b>43</b> | <b>30</b> | <b>27</b> | 39 | 36 | 12 | 38 | 29 | 24 | 51 | ammonium, carbon, nitrate |
| 13 | 1,654 | <u>30</u> | <u>18</u> | <b>12</b> | 27        | 43        | 37 | 36 | 24 | 39 | 29 | 17 | 28 | nitrate, ammonium, carbon |
| 14 | 1,623 | <u>51</u> | <b>67</b> | 27        | 37        | 18        | 43 | 36 | 39 | 23 | 30 | 12 | 38 | vanadium-rich, carbon     |
| 15 | 1,561 | <u>56</u> | 39        | 57        | 40        | 27        | 23 | 54 | 2  | 1  | 51 | 41 | 24 | iron-rich dust            |
| 16 | 1,493 | <u>36</u> | <b>12</b> | 37        | 24        | 27        | 43 | 18 | 30 | 39 | 48 | 23 | 60 | elemental carbon          |
| 17 | 1493  | <u>12</u> | <b>36</b> | <b>24</b> | 27        | 37        | 18 | 30 | 43 | 29 | 39 | 28 | 17 | elemental carbon          |
| 18 | 1424  | <u>2</u>  | <b>16</b> | <b>23</b> | <b>27</b> | 39        | 25 | 24 | 26 | 28 | 40 | 29 | 41 | soil dust                 |
| 19 | 1264  | <u>2</u>  | <u>24</u> | <b>27</b> | 28        | 17        | 40 | 16 | 29 | 39 | 26 | 25 | 41 | soil dust                 |
| 20 | 1229  | <u>2</u>  | <b>25</b> | <b>17</b> | <b>28</b> | 23        | 27 | 40 | 24 | 29 | 26 | 41 | 16 | soil dust                 |

### 2.3.2 Chemical Composition of the Particle Classes Determined by ART-2a Analysis

The top 20 weight vectors from the ART-2a analysis are shown in Figures 2.2-2.4, in the form of normalized intensity versus  $m/z$ . Larger versions of the weight matrices are included in Appendix C. The weight vectors represent the mass spectra when normalized and reduced to unit mass resolution. Although values up to 350  $m/z$  were considered in the ART-2a analysis, the range plotted for each weight vector is truncated to highlight the range where many of the characteristic peaks are prevalent, the first 100  $m/z$  units of the positive ion mass spectra.

The normalized weight vectors for eight clusters that have characteristic organic carbon marker peaks are presented in Figure 2.2. Clusters 4, 8, 11, 12, 13, 14, 16, and 17 have organic and elemental carbon fragment peaks at  $m/z$  12, 15, 27, 29, 36, 37, and 43. Combustion processes, dominated by vehicle exhaust, are the most common source of sub-micron carbonaceous particles in southern California. In addition, while moving across the inland valleys of southern California to Riverside, particles can accumulate organic carbon species from a variety of sources as well as undergo secondary processing to form secondary organic aerosols (SOA). The weight vectors for clusters 4 and 11 show a peak at  $m/z$  86. Based on smog chamber experiments, the most likely assignment for this peak is  $^{86}[(C_2H_5)_2 N=CH_2]^+$ , a commonly observed fragment of alkylamines. Along a typical air southern California mass trajectory from Los Angeles to Riverside, an air mass passes across areas of freeway traffic and dairies, possible sources of this particle type (Angelino 2001). Cluster 16 and 17 possess distinct elemental carbon signatures, similar to those observed from both diesel and newer gasoline vehicles. Carbon peaks, including  $^{12}C^+$ ,  $^{24}C_2^+$ , and  $^{36}C_3^+$  are among the most intense for particles in these

two elemental carbon clusters. Clusters 16 and 17 will be considered together as elemental carbon because they have similar composition as well as size and temporal profiles. Peaks at  $m/z$  18 and 30 appear in the cluster of each “organic” weight vector. The particles in clusters 8 and 13 have  $m/z$  18 and 30 as their most intense peaks, indicating the presence of ammonium  $^{18}(\text{NH}_4)^+$  and nitrate  $^{30}(\text{NO})^+$ , a fragment of nitrate. Ammonium nitrate enriched particles are observed quite commonly in Riverside (Song 1999; Liu 2000). The particles in clusters 8 and 13 may have evolved from the secondary coating of sub- $\mu\text{m}$  carbon particles with ammonium nitrate, generated by a gas-to-particle reaction such as:  $\text{NH}_3(\text{g}) + \text{HNO}_3(\text{g}) \rightarrow \text{NH}_4\text{NO}_3(\text{s})$ . Particles in cluster 12 also have a strong ammonium nitrate signature blended with organic carbon. Finally, the weight vector for cluster 14 contains peaks similar to clusters 4 and 11, as well as vanadium and vanadium oxide peaks,  $^{51}\text{V}^+$  and  $^{67}(\text{VO})^+$  (Figure 2.2h).

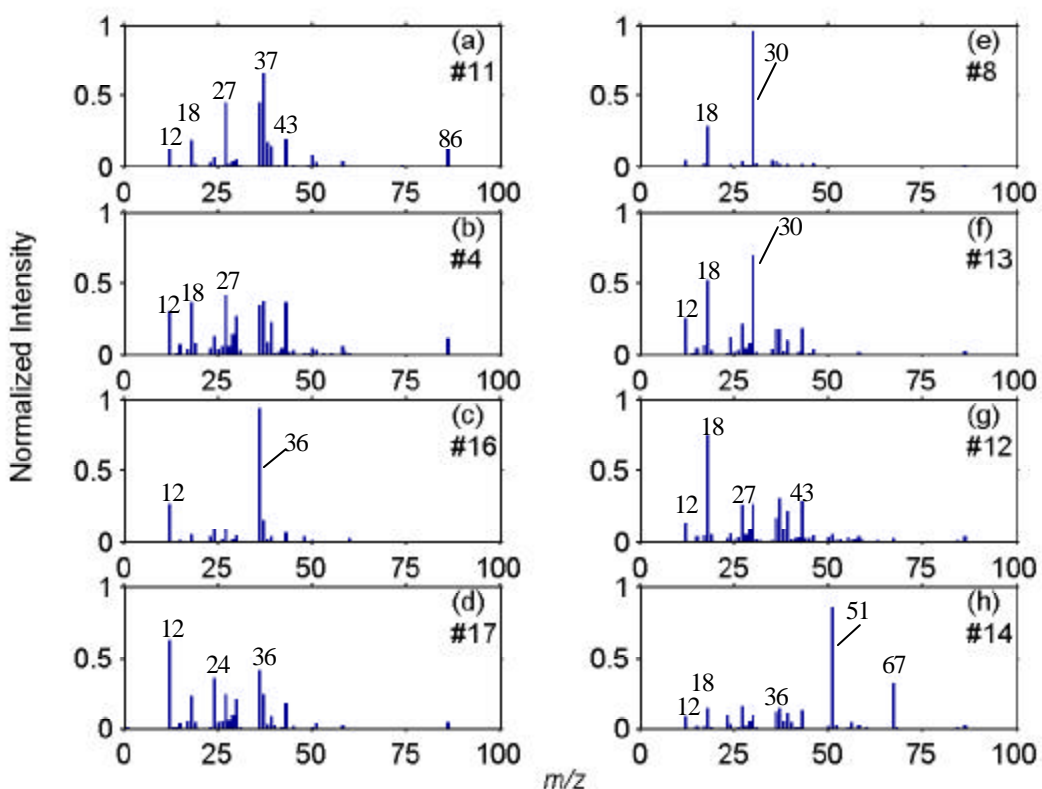


Figure 2.2: Normalized weight vectors for common organic carbon particle classes identified by ART-2a: (a) cluster 11 organic carbon with amines I, (b) cluster 4 organic carbon with amines II, (c) cluster 16 elemental carbon I, (d) cluster 17 elemental carbon II, (e) cluster 8 ammonium nitrate I, (f) cluster 13 ammonium nitrate II, (g) cluster 12 ammonium nitrate III, and (h) cluster 14 vanadium-rich.

Clusters 1, 2, 3, 5, 6, 7, 9, and 15 have a range of distinct inorganic signatures (Figure 2.3). Particles in clusters 1 and 2 are sea salt particles. Sea salt type particles are commonly detected in Riverside, located about 60 miles east of the Pacific coast (Song 1999). The mass spectral markers for sea salt include  $^{23}\text{Na}^+$ ,  $^{39/41}\text{K}^+$ ,  $^{40}\text{Ca}^+$ ,  $^{62}(\text{Na}_2\text{O})^+$ ,  $^{108}(\text{Na}_2\text{NO}_3)^+$  and  $^{165}(\text{Na}_3\text{SO}_4)^+$ .

While the weight vectors of clusters 1 and 2 have several features in common, they were distinguished as unique classes by ART-2a. Ion peaks at  $m/z$  108 and 165 are more prominent for particles in cluster 2. The presence of peaks at  $m/z$  108 and 165 in the weight vector indicates that many of the particles in this cluster had undergone reactions with gas phase  $\text{NO}_x$  and  $\text{SO}_x$  species (Gard 1998). These differences in the weight vectors of clusters 1 and 2 indicate that cluster 2 is a more reacted or aged form of sea salt than cluster 1. Calcium marker peaks,  $^{40}\text{Ca}^+$ , and  $^{57}(\text{CaOH})^+$ , are among the most intense peaks for clusters 3 and 6. A high number of Ca-containing particles were observed in previous studies in nearby Rubidoux (Chow 1992; Chow 1994; Kim 2000; Kim 2000). Despite the similarity in the chemical signatures, the temporal trends of calcium-rich clusters 3 and 6 are quite different, further supporting the assignment by ART-2a as two unique calcium-rich classes. Cluster 15 contains peaks that are generally classified as dust, including  $^{23}\text{Na}^+$ ,  $^{27}\text{Al}^+$ , and  $^{39}\text{K}^+$ , and calcium-rich  $^{40}\text{Ca}^+$  and  $^{57}(\text{CaOH})^+$  (Silva 2000). The peak for iron,  $^{56}\text{Fe}^+$ , dominates the weight vector for cluster 15 indicating these particles are iron-rich. The particles in clusters 5, 7, and 9 have  $^{39}\text{K}^+$  as the most intense peak. These clusters are classified as potassium-rich dust. Since the size and temporal profiles for clusters 5 and 7 are similar as well as their composition, they are grouped together. However, cluster 9 has a different temporal profile, particularly on August 21, and thus was not grouped with clusters 5 and 7.

Figure 2.4 shows the normalized weight vectors of four other inorganic particle clusters: 10, 18, 19, and 20. These weight vectors often have peaks at 23, 27, 39, and 40 and have the most intense peak at  $m/z$  1 or 2 (due to miscalibration). The peaks in these spectra are wide with non-Gaussian shapes, leading to miscalibrated peaks for clusters 18, 19, and 20. Because they have similar size and temporal profiles and the peaks are just shifted by one  $m/z$  unit, the particles in clusters 10, 18, 19, and 20 are merged together and labeled as soil dust.

As an extension of this analysis, the similarity among the Riverside ambient clusters can be examined (Figure 2.5; Appendix P shows color version). The degree of similarity between the clusters can be calculated and plotted. The dot product of the weight vectors is used for this comparison. As verification, when the comparison is made between the Riverside weight matrix and itself, the dot product for a weight vector and itself should be exactly 1. Since the value of the dot product for a pair of clusters will indicate the similarity and the grayscale shading of the plot indicates the dot product value, the shading in the plot is a way to visualize the similarity between any 2 clusters in this set.

In the resulting plot, the dot product is represented in grayscale. A bright white square appears where each weight vector is compared to itself, forming a diagonal from the upper left to lower right and this is demonstrated (Figure 2.5). The weight vectors for the Riverside ambient classes (vigilance factor of 0.5) are compared to one another in the remainder of the matrix and plot. The lighter (more white) squares indicate higher similarity and the darker squares indicate lower similarity. For example, the dot product was 0.8601 for clusters 4 and 11, which were grouped together as organic carbon with ammonium and nitrate. As a second example, the three clusters in the lower right corner of the plot, clusters 18-20, were considered together as soil dust. They have a similarity (dot product of weight vectors) of  $\sim 0.8$  with one another. The pairings/groupings of particle classes discussed earlier in this section are confirmed in this analysis.

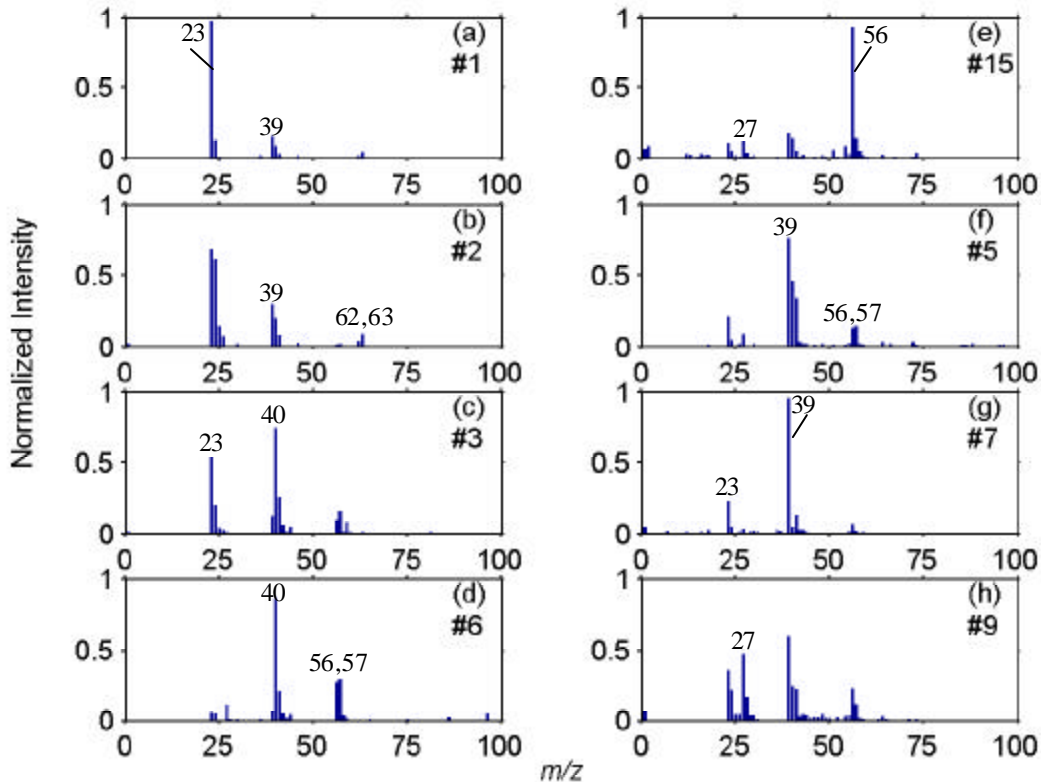


**Figure 2.3:** Normalized weight vectors for common inorganic particle classes identified by ART-2a: (a) cluster 1 sea salt I, (b) cluster 2 sea salt II, (c) cluster 3 calcium-rich I, (d) cluster 6 calcium-rich II, (e) cluster 15 iron-rich, (f) cluster 5 potassium-rich I, (g) cluster 7 potassium-rich II, and (h) cluster 9 potassium-rich III.

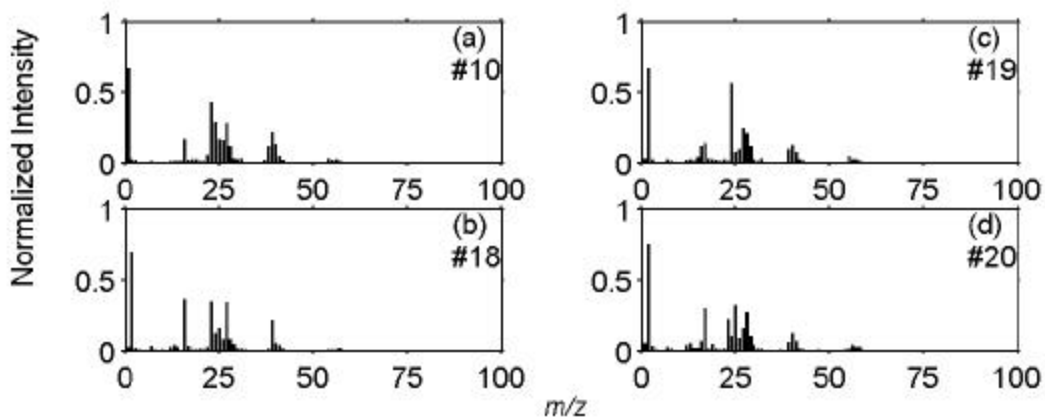


**Figure 2.4:** Normalized weight vectors for common soil dust particle classes identified by ART-2a: (a) cluster 10, (b) cluster 18, (c) cluster 19, and (d) cluster 20.

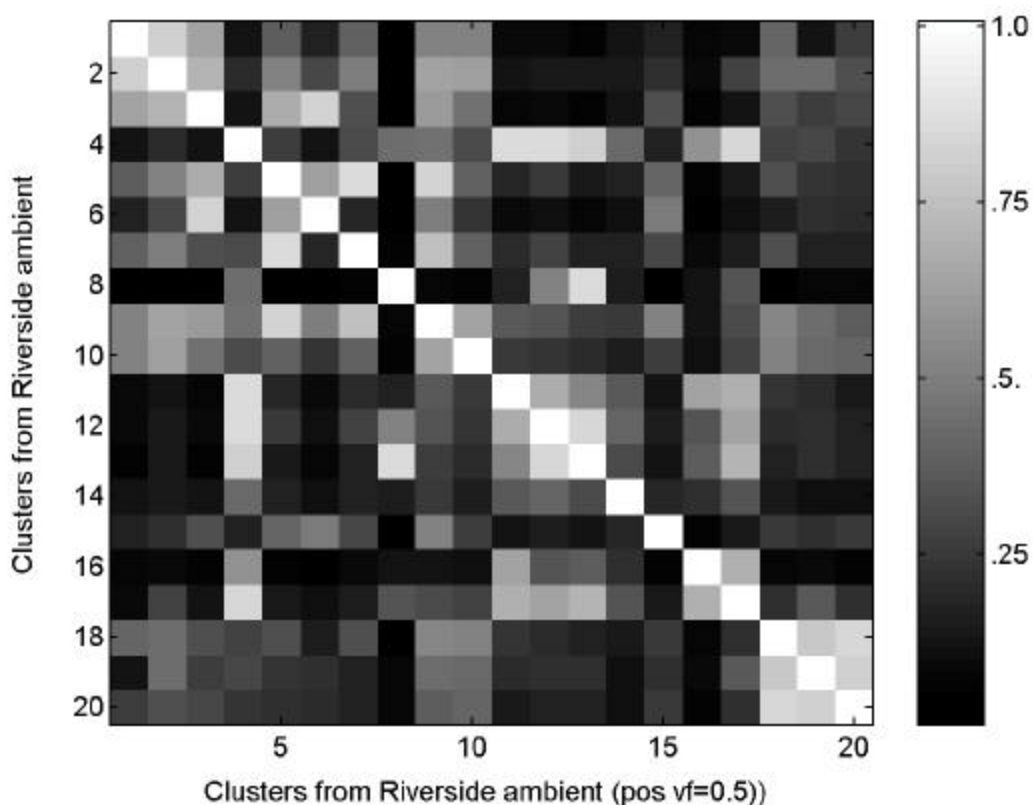


**Figure 2.5: Similarity plot for weight matrices from Riverside ambient and itself (vigilance factor 0.5).**

### 2.3.3 Size Distributions of Particle Classes Determined by ART-2a

Figures 2.6-2.7 show the size profiles of organic and inorganic clusters, respectively. For these plots, as well as Figures 2.10-2.11, the histograms are not scaled for instrumental transmission/detection efficiency, since relative differences between the times periods are more apparent with the unscaled ATOFMS data. Examples of scaled ATOFMS data are shown in Figure 2.14. The particles detected by the instrument tend to be centered either above or below 1  $\mu\text{m}$ . This well-defined break is consistent with previous studies conducted in southern California (Noble 1996; Hughes 1999; Song 1999; Hughes 2000; Hughes 2002), as well as other locations (Kegler 2001; Thomas 2002; Wilson 2002). The size profiles are plotted with 0.1- $\mu\text{m}$  resolution for the range 0.5 to 2.5  $\mu\text{m}$ .

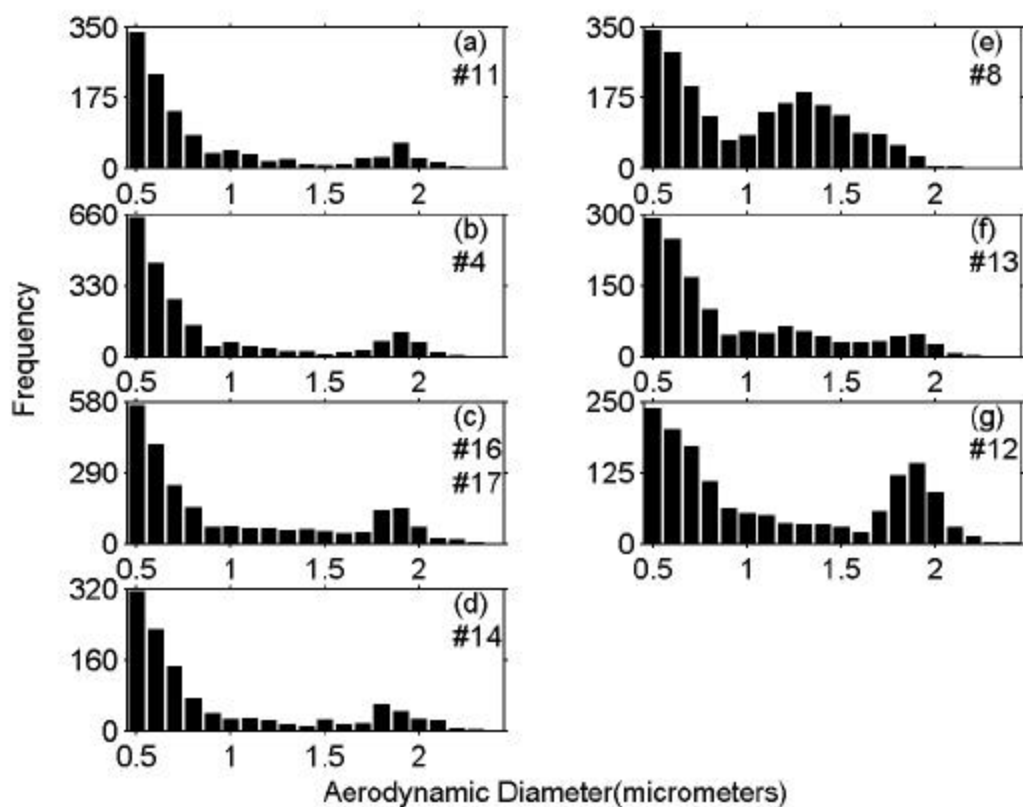


**Figure 2.6: Size distribution plots for common organic particle classes identified by ART-2a: (a) cluster 11 organic carbon with amines I, (b) cluster 4 organic carbon with amines II, (c) grouped clusters 16 and 17 elemental carbon, (d) cluster 14 vanadium-rich (e) cluster 8 ammonium nitrate I, (f) cluster 13 ammonium nitrate II, and (g) cluster 12 ammonium nitrate III.**

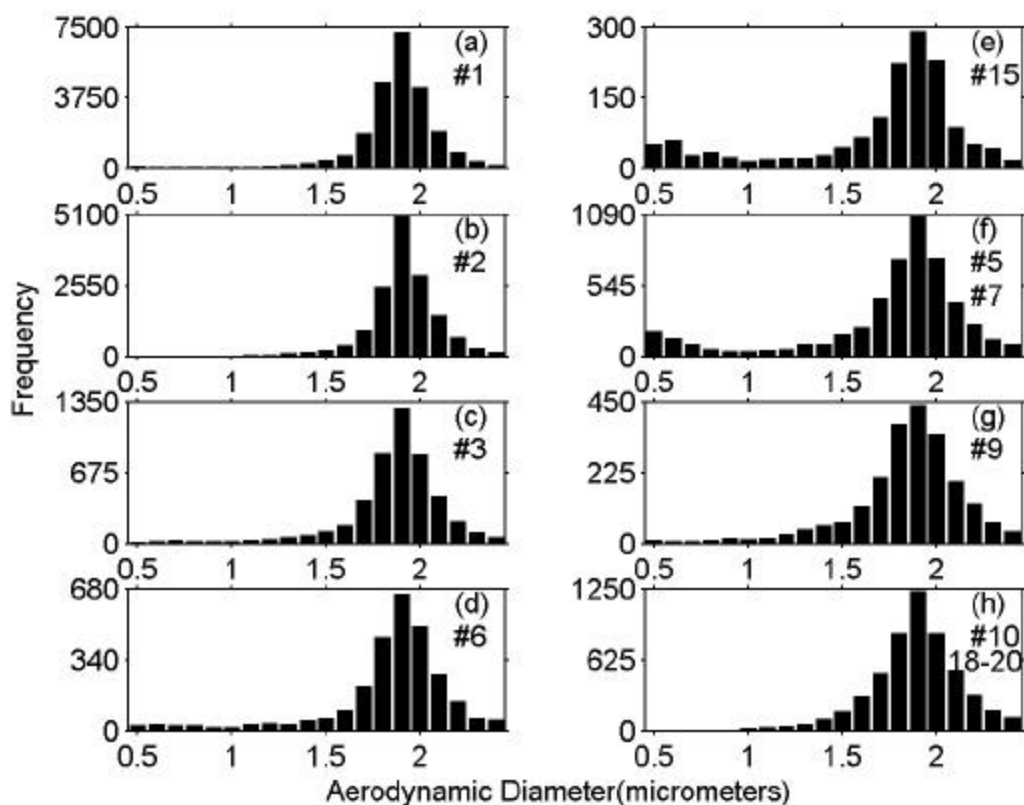


**Figure 2.7: Size distribution plots for common inorganic particle classes identified by ART-2a: (a) cluster 1 sea salt I, (b) cluster 2 sea salt II, (c) cluster 3 calcium-rich I, (d) cluster 6 calcium-rich II, (e) cluster 15 iron-rich, (f) grouped clusters 5 and 7 potassium-rich, (g) cluster 9 potassium-rich III, and (h) grouped clusters 10, 18, 19, and 20 soil dust.**

The size histograms for the common organic clusters show a large number of the particles have aerodynamic diameters of less than 1  $\mu\text{m}$  (Figure 2.6). The size profile for cluster 8 is uniquely bimodal (Figure 2.6e). The super- $\mu\text{m}$  particles in cluster 8 appear in a narrow time range on August 23, peaking at about 10:00, as noted previously by Liu et al. in a publication describing nitrate-containing particles in Riverside, CA (Liu 2000). The particles in cluster 12 are mostly super- $\mu\text{m}$  and occur during the late afternoon of August 21 (Figure 2.6g). In this case, from the single particle data, the coarse mode ammonium is associated with nitrate in OC particles and not with wind-blown soil, a possible scenario suggested by John et al. in a previous study (John 1990). The vanadium-rich particles are sub- $\mu\text{m}$ , as observed in other studies in southern California as well as other countries (Cahill 1996; Singh 2002; Thomas 2002). The size histograms of the common inorganic clusters are super- $\mu\text{m}$ , and most likely the lower size end of mechanically-generated (coarse) particles (Figure 2.7). In summary, the size profiles show particles of organic carbon, elemental carbon, and ammonium nitrate types primarily in the sub- $\mu\text{m}$  range. In contrast, the sea salt, inorganic-enriched dusts, and soil dust particle types occur primarily in the super- $\mu\text{m}$  range. These size profiles suggest that a  $\text{PM}_{1.0}$  standard could generally distinguish combustion generated particles (EC, OC) from sea salt and dust in the

Riverside aerosol, as the composition changes significantly around 1  $\mu\text{m}$ , a finding that is consistent with a number of other previous studies.

### 2.3.4 Temporal Characteristics of Riverside Air Quality

The temporal characteristics of Riverside's air quality can be described by taking into account ozone,  $\text{PM}_{10}$ ,  $b_{\text{scat}}$ , wind trajectory, and ATOFMS data. The hourly ozone,  $\text{PM}_{10}$ , and  $b_{\text{scat}}$  data are shown in Figure 2.8. Hourly  $\text{PM}_{2.5}$  data were not available for Riverside during this period. Four daily  $\text{PM}_{2.5}$  measurements were available, 23.5 hour averages starting at 10:00. The average values for August 21, 22, and 23 were 13, 28, and 24  $\mu\text{g m}^{-3}$ , respectively. The temporal profiles of the most common ATOFMS particle classes are shown in Figures 2.10 and 2.11. The trajectory plots for six time periods are shown in Figure 2.9.

The hourly average ozone in Riverside on August 21-23, 1997 peaked each afternoon (Figure 2.8). Each morning, the hourly  $\text{PM}_{10}$  level peaked and a second, smaller  $\text{PM}_{10}$  peak occurred each afternoon. An afternoon peak in the  $b_{\text{scat}}$  and  $\text{PM}_{10}$  data coincided with the daily ozone peak. The  $\text{PM}_{10}$  values rose each morning while the ozone levels remained low. The  $b_{\text{scat}}$  values show a peak each morning, a larger peak each afternoon, and an additional peak at 1:00 on August 23. It is interesting to note that the  $b_{\text{scat}}$  peak on the morning of August 22 was the smallest peak in the 3-day period yet the  $\text{PM}_{10}$  levels were at their highest. The ATOFMS data can be used to help explain this observation by identifying the types of particles that were present.

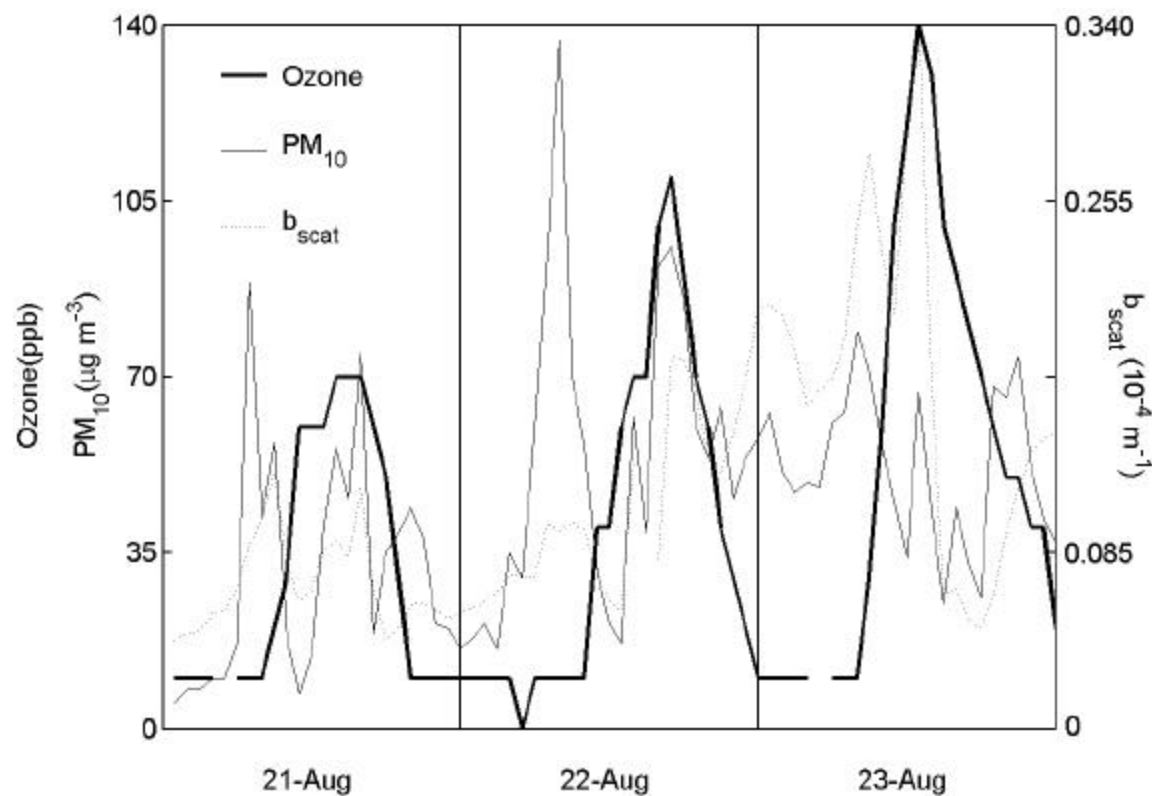


**Figure 2.8: Time series plots for hourly ozone,  $\text{PM}_{10}$ , and  $b_{\text{scat}}$  measurements for Riverside, August 21-23, 1997 (note the two y-axes).**

Based on the ambient data, six time periods of interest were chosen. Three afternoon periods of high ozone levels occurred on August 21 14:00-16:00, August 22 17:00, and August 23 13:00 during which the  $b_{\text{scat}}$  values also increased. Three time periods with low ozone levels and high  $\text{PM}_{10}$  levels occurred on August 21 7:00, August 22 8:00, and August 23 8:00. The average morning ozone level was only 10 ppb but the afternoon average was over 100 ppb. The average morning  $b_{\text{scat}}$  was  $0.14 \times 10^{-4} \text{ m}^{-1}$  and the afternoon average was  $0.20 \times 10^{-4} \text{ m}^{-1}$ . The average morning  $\text{PM}_{10}$  peak was about  $100 \mu\text{g m}^{-3}$  and the afternoon average was  $70 \mu\text{g m}^{-3}$ .

Trajectory plots for the six time periods of interest are shown in Figure 2.9, indicating the paths of the air masses. The open circles represent the location of the air parcel at consecutive hours for 60 hours before the air mass arrived in Riverside. Overlapping circles indicate stagnation of the air parcel, which usually occurred overnight between about 20:00 and 10:00 and sometimes for longer periods of time. On August 21, air parcels had come from over the Pacific and east of Catalina Island. On August 22 and 23, the trajectory plots show the air masses arriving from over the Pacific, north of Catalina Island. Some air masses stagnated near the Mira Loma area that has dairies and elevated levels of gas phase ammonia (Russell 1988; Solomon 1988). The trend from August 21-23 is that air masses spend more and more time over land. It can be immediately noted that the August 23 air masses spent the most time over land because almost all of the 60 data points shown on August 23 are over land. These air masses spending more and more time over land is consistent with the increasing daily ozone peak concentrations observed August 21-23 and would be consistent an increased presence of pollution-derived particles due to stagnant meteorological conditions.

The ATOFMS size profiles of the particles in Riverside at the times of interest generally show two modes. One mode occurs between 1.5 and 2.5  $\mu\text{m}$  and a second mode below 1  $\mu\text{m}$ . It is important to note that during the afternoon, elevated-ozone time periods show a larger contribution from particles in the sub-  $\mu\text{m}$  mode relative to those in the super-  $\mu\text{m}$  mode. This is consistent with the optical particle counter and particle filter sample data. The optical particle counter data show an increase in the sub-  $\mu\text{m}$  particle mass concentration in the afternoons, particularly between 0.5 and 1  $\mu\text{m}$ , accompanied by a decrease in the super-  $\mu\text{m}$  particle mass concentration. Also the fine (<1.9  $\mu\text{m}$ ) and coarse (<10  $\mu\text{m}$ ) particle filter samples, collected by the Cass research group on August 21 and 22 in Riverside, show slightly higher morning coarse particle concentrations and a doubling of the fine particle concentration between the morning and afternoon of August 21. The particle size distribution clearly shifts between the mornings and the afternoon periods. The ATOFMS data show simultaneous particle composition changes that further explain the changes in visibility. The temporal plots of the various particle-composition types show when each of the particle types was detected.

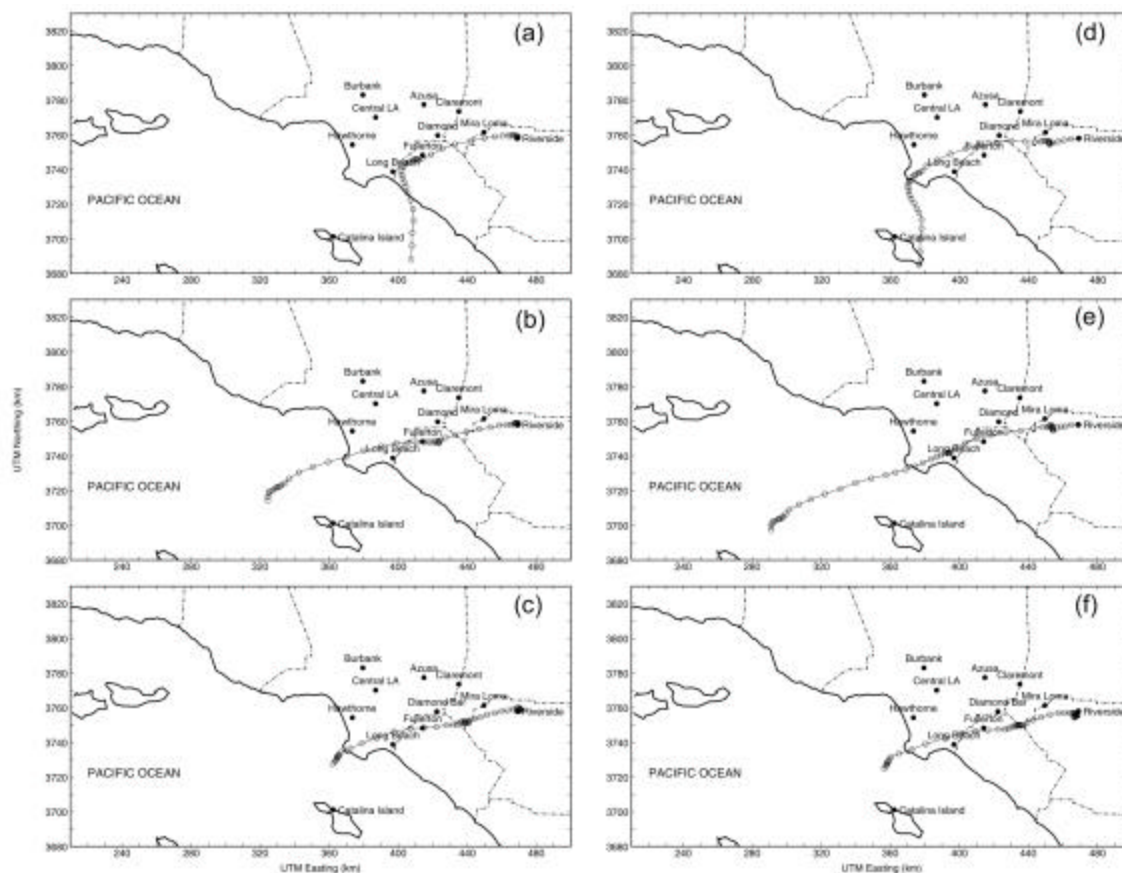


**Figure 2.9: Representative air parcel trajectory arriving at Riverside, CA during elevated  $PM_{10}$  at: (a) 7:00 August 21, 1997, (b) 8:00 August 22, 1997, (c) 8:00 August 23, 1997, and elevated ozone at: (d) 16:00 August 21, 1997 (d) 17:00 August 22, 1997(d) 13:00 August 23, 1997.**

The temporal profiles of the organic and inorganic clusters are presented in Figure 2.10 and Figure 2.11, respectively, with 30-minute temporal resolution. If the ATOFMS instrument collected positive ion mass spectra for less than 24 of the 30 minutes (i.e. offline for greater than 20% of the time), no data are plotted. For all remaining time periods, the ATOFMS data were scaled upward to estimate the actual number of particles that would have been acquired in a full half-hour period to account for the small amount of offline time in any given period. Figure 2.10 shows the temporal histograms for the organic clusters: 4, 8, 11, 12, 13, 14, and 16/17. Figure 2.11 shows the temporal histograms for the inorganic clusters: 1, 2, 3, 6, 9, 15, 5/7, and 10/18/19/20. The temporal trend of the  $PM_{10}$  or ozone is plotted with each cluster's temporal profile. It is important to note the afternoon  $PM_{10}$  and  $b_{scat}$  peaks generally coincide with the ozone peak. From examining these plots, one can determine the particle types that correlate with the ozone levels versus the  $PM_{10}$  levels.

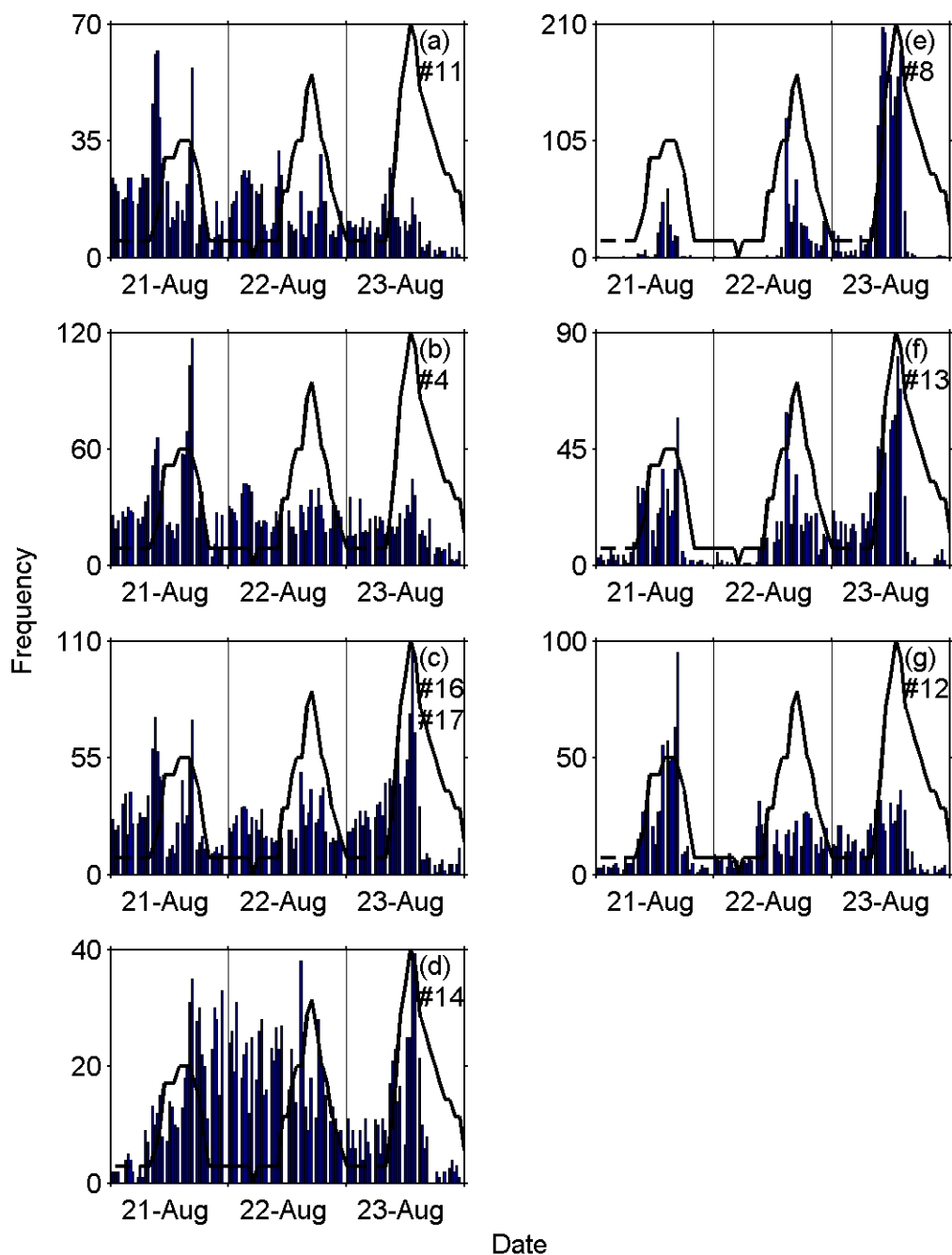


**Figure 2.10: Time series plots of common organic particle classes identified by ART-2a: (a) cluster 11 organic carbon with amines I, (b) cluster 4 organic carbon with amines II, (c) grouped clusters 16 and 17 elemental carbon, (d) cluster 14 vanadium-rich, (e) cluster 8 ammonium nitrate I, (f) cluster 13 ammonium nitrate II, and (g) cluster 12 ammonium nitrate III with the temporal trend ozone overlaid. Temporal resolution is 30 min for the single particle data and 60 min for the ozone data.**

Cluster 13 most closely tracks the temporal profile for ozone (Figure 2.10f), while cluster 8 has the next closest correlation (Figure 2.10e). A larger sub- $\mu\text{m}$  mode of ammonium-nitrate-organic carbon particles appears during the periods of elevated ozone in the afternoon. These midday peaks in fine particle nitrate are consistent with data from previous field campaigns in southern California (John 1990; Wexler 1992). Clusters 8 and 13 particles are only present when the ozone levels are high. Furthermore, it is important to note that these particle types disappear immediately when the marine layer arrives in Riverside, particularly on the afternoon of August 23<sup>rd</sup> which is evident upon comparison of Figures 2.10e and 2.10f with Figures 2.11a and 2.11b, respectively (see Figure 2.12 for temporal profiles for clusters 1, 2, 8 and 13 plotted together). It is interesting to note that the visibility levels increase dramatically when the marine layer arrives and clusters 8 and 13 disappear, however the ozone levels decrease much more slowly. The correlation observed between clusters 8 and 13 and ozone is the strongest gas-particle trend observed with ATOFMS during this study. One possible explanation for the observed gas and particle phase correlations could be that typical ambient air in Riverside is composed of an excess of gas phase ammonia, and thus the formation of ammonium nitrate is limited by the availability of nitric acid. This is consistent with other studies in the Riverside area, including one performed later in 1997 (Lurmann 1997; Hughes 2002). The ozone concentrations could be serving as a surrogate measure of the ambient nitric acid levels, which means as the ozone levels increase so do the nitric acid levels, producing an increase in the numbers of particles containing significant amounts of ammonium nitrate (clusters 8 and 13).

The wind trajectories for the afternoon periods on August 21 and 22 show the air parcels stagnated over land near Mira Loma before reaching Riverside (Figure 2.9d-e), and thus the arriving air masses had a significant dairy-influence from stagnation. The trajectory for the air mass arriving during the largest ozone peak in the 3-day period, on August 23, stagnated over Riverside for about 18 hours (Figure 2.9f). The rapid appearance of the ammonium-nitrate-organic carbon particles coupled with the stagnant nature of the air masses indicate that this chemistry is occurring in Riverside and not being transported in from another location. During this extended stagnation episode on August 23, the particles grew through condensation and agglomeration processes giving a unique size distribution with a small peak halfway between the sub- and super- $\mu\text{m}$  particles. The ATOFMS results indicate the ammonium-nitrate-organic carbon particles are responsible for the decreased visibility in Riverside during this time period. In fact, looking closely at the  $b_{\text{scat}}$  profile, one notices a peak in the  $b_{\text{scat}}$  just before the ozone peak, corresponding to an increase in the ammonium-nitrate-organic carbon particles. Furthermore, as previously described, when these particles disappear upon arrival of the marine front, the  $b_{\text{scat}}$  values immediately decrease as well. The strong relationship between this particle type and visibility reduction may add to our understanding of the specific particle types that have the strongest influence on atmospheric visibility (Watson 2002).

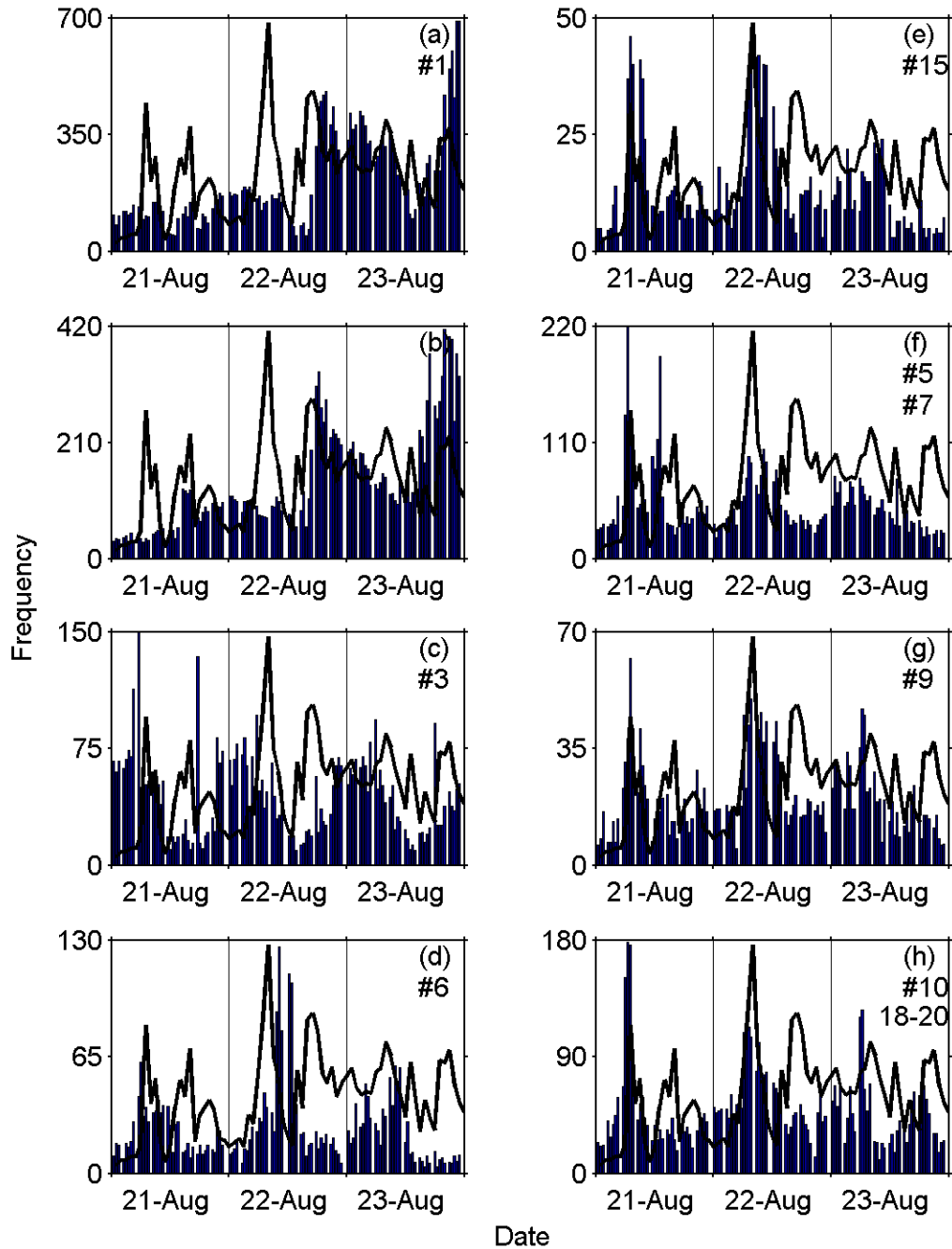


**Figure 2.11: Time series plots for common inorganic particle classes identified by ART-2a: (a) cluster 1 sea salt I, (b) cluster 2 sea salt II, (c) cluster 3 calcium-rich I, (d) cluster 6 calcium-rich II, (e) cluster 15 iron-rich, (f) grouped clusters 5 and 7 potassium-rich, (g) cluster 9 potassium-rich III, and (h) grouped clusters 10, 18, 19, and 20 soil dust with the temporal trend of  $PM_{10}$  overlaid. Temporal resolution is 30 min for the single particle data and 60 min for the  $PM_{10}$  data.**

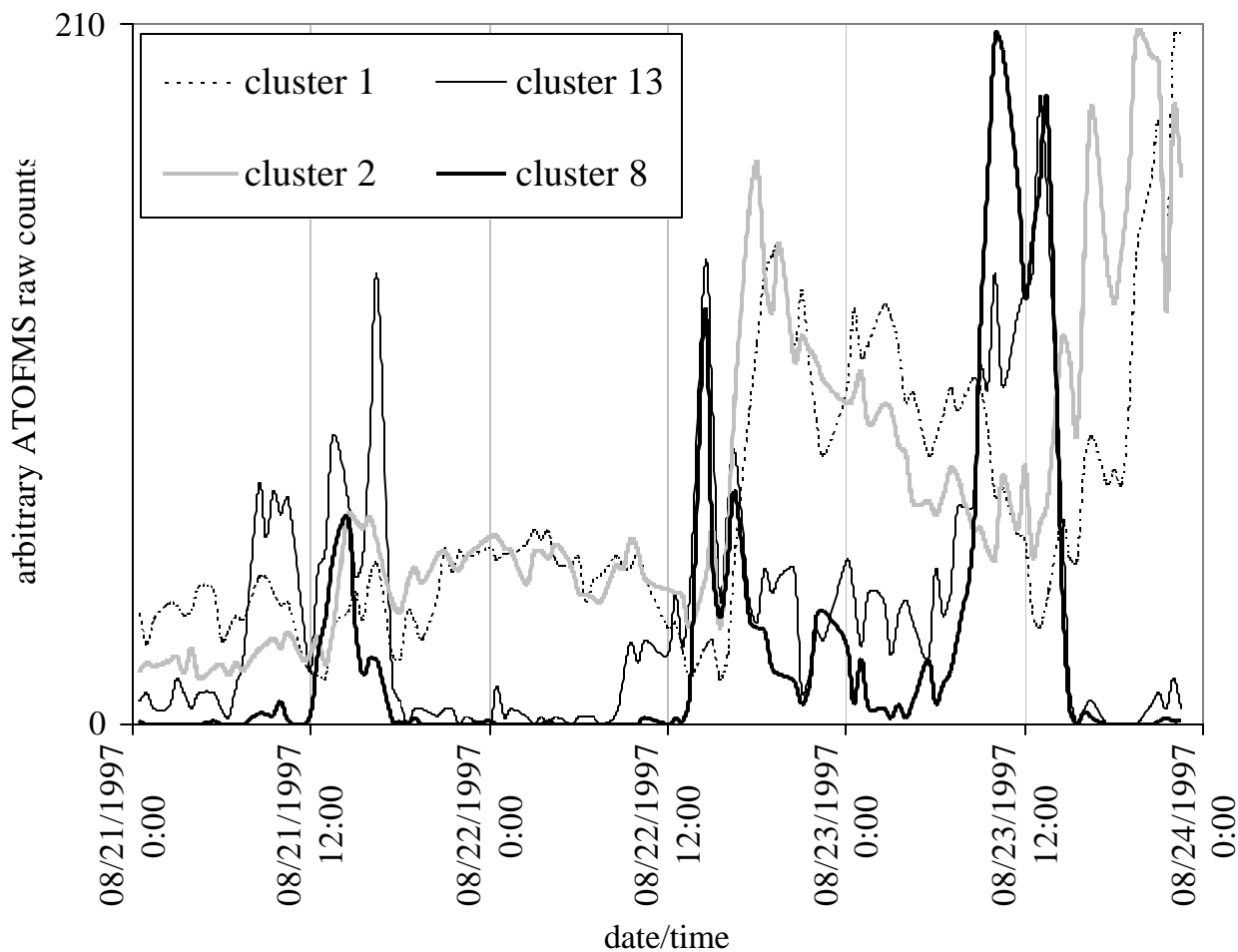


**Figure 2.12: Time series plots for common particle classes identified by ART-2a: cluster 1 sea salt I, cluster 2 sea salt II, cluster 8 ammonium nitrate I, and cluster 13 ammonium nitrate II. Temporal resolution is 30 min for the single particle data.**

The temporal profiles of the inorganic clusters do not peak with ozone but instead track the morning  $PM_{10}$  concentrations (Figure 2.11). The particles in the sea salt classes peak just after the ozone level maxima on all 3 days (Figure 2.11a-b), marking the arrival of cleaner air. The wind trajectories show that sea salt enriched air masses arriving in Riverside, such as August 22, 1997 20:00 (Figure 2.13) stagnated at the coast before making landfall, explaining the dominance of sea salt particles. Following the stagnation period at the coast, the estimated time over land for this sea salt enriched air mass was relatively short. The air mass traveled quickly over land leaving little time for the particles to become transformed by land-based emissions. The fresh marine air mass replaced the polluted afternoon air mass that had stagnated for many hours in Riverside.

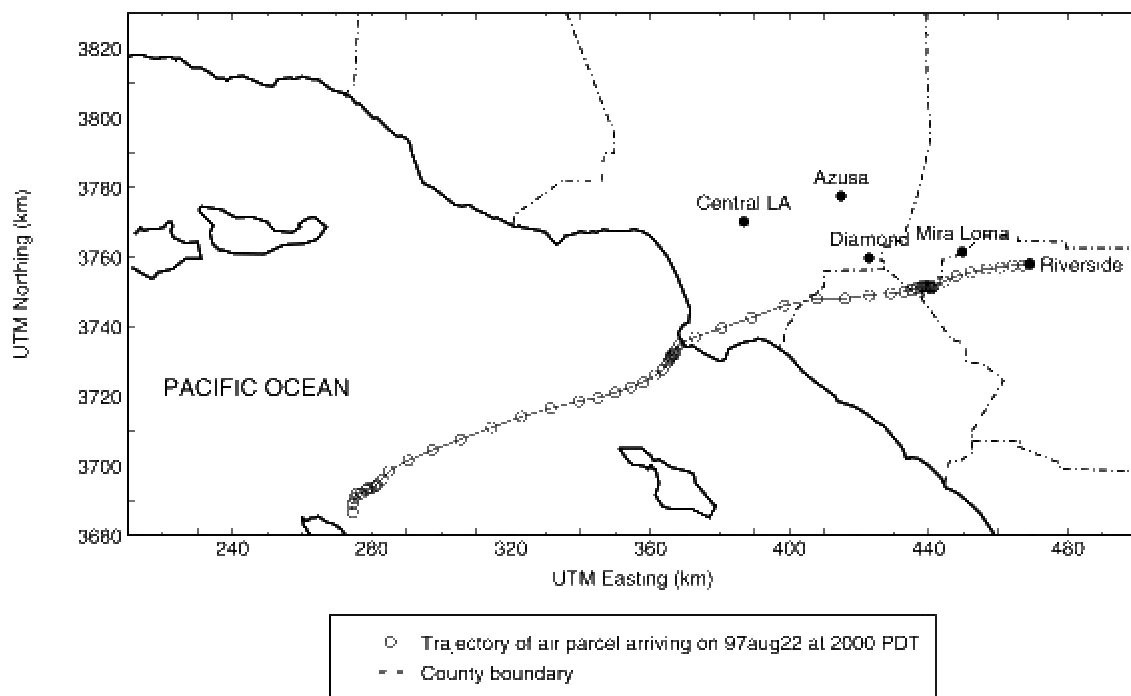


**Figure 2.13: Air parcel trajectory arriving at Riverside, CA 20:00 August 22, 1997. Note the air mass stagnation at the coast before landfall.**

One of the calcium-rich particle types, cluster 3, shows a strong diurnal variation, peaking each morning around 3:00. Its presence is generally anti-correlated with ozone (Figure 2.11c). A local source of these calcium-rich particles is the most logical explanation for this type of particle because the wind trajectories show no significant movement during these times. With substantial ion signals due to calcium, cluster 6 is similar to cluster 3, however the particles in cluster 3 contain more sodium. The temporal profiles of these clusters are different, indicating different sources (Figure 2.11c-d). The soil and metal-rich dust particles peak in number during the morning PM<sub>10</sub> peaks (Figure 2.11e-h). The temporal profile of cluster 6 is similar to the temporal profile of soil dust suggesting the cluster 6 particles may be of crustal/soil origin (Figure 2.11d,h). Inorganic particle types dominate the large super- $\mu\text{m}$  mode observed during the morning periods with elevated PM<sub>10</sub> levels.

### 2.3.5 Scaled Size Distributions with Particle Composition

The ATOFMS mass spectral and particle-size data can be used to provide a summary of the size-composition relationships of the individual particles as shown in Figure 2.14. The particles were grouped into broader particle types based on the class descriptions in Table 1 to generate the composition information within the bars of size histograms. These clusters have similar size profiles and are grouped by general composition in order generate the pattern-coding for Figure 2.14. Classes 1 and 2 are labeled sea salt; classes 3 and 6 are calcium-rich; classes 4 and 11 are organic carbon with amines; classes 5, 7, and 9 are potassium-rich; classes 8, 12, and 13 are organic carbon with ammonium nitrate; class 10, 18, 19, and 20 are soil dust; class 16 and 17 are elemental carbon; class 14 is vanadium-rich, and class 15 is iron-rich. The particles in

these classes account for over eighty-five percent of the total particles and eighty percent or more of the particles in each time period plotted. The remainder of the particle population, the particles in the less common classes (clusters 21-57), are omitted from Figure 2.14 to simplify the plot.

The size distributions for the morning periods with elevated  $PM_{10}$  and low ozone levels are represented by the average of the ATOFMS data from August 21 at 7:00, August 22 at 8:00, and August 23 at 8:00. The afternoon periods with elevated levels of ozone,  $PM_{10}$ , and  $b_{scat}$ , are represented by an average of the ATOFMS data from August 21 at 15:00, August 22 at 17:00, and August 23 at 13:00. The plot for each time period has been separated into two size ranges to allow the presentation of data over a large concentration range. The scaled number concentration for 0.4 to 0.9  $\mu m$  particles appear in Figure 2.14a-b, while the scaled number concentration information for 0.9 to 2.5  $\mu m$  particles appear in Figure 2.14c-d. The y-axes are shown with the same range for the two time periods to allow for visual comparison of the data. The representative number concentrations were generated from the ATOFMS data using the detection-efficiency calibration function which was calculated by comparison of seven pairs of ambient Riverside aerosol ATOFMS and MOUDI data sampled during SCOS97-NARSTO (Figure 2.14).

Each day was unique, but similar general trends were observed. The trends are consistent in both the unscaled and scaled ATOFMS data. The individual particles in Riverside are significantly different between the morning and afternoon periods. The morning periods were characterized by the presence of sea salt, metal-rich-dust, and soil-dust particles in the super- $\mu m$  mode. In contrast, the afternoon ozone episodes were characterized by sub- $\mu m$  particles composed of organic carbon, elemental carbon, ammonium, nitrate, and amines. Based on single particle mass spectra, sea salt and soil dust account for a significant fraction of the particulate matter mass in Riverside, including when the highest  $PM_{10}$  level of almost  $140 \mu g m^{-3}$  was reached in Riverside. Based on the ATOFMS data, in addition to contributing to  $PM_{10}$  mass, sea salt and dust particles contribute to the mass of particulate matter below 2.5  $\mu m$  ( $PM_{2.5}$ ). This is consistent with observations of soil in the  $PM_{2.5}$  fraction in Phoenix (Keglar et al., 2001). Therefore, we also conclude that the current  $PM_{2.5}$  regulation would not allow one to distinguish between anthropogenic and biogenic particle sources because the composition shift is observed around 1  $\mu m$ . These findings also highlight presence of soil and sea salt as components of the southern California particulate matter pollution. Particulate matter episodes and most of the pollution burden in southern California are often attributed solely to the many industries and vehicles present. In this study, natural sources such as sea salt and soil also make substantial contributions to the  $PM_{10}$  (and  $PM_{2.5}$ ) mass concentrations.

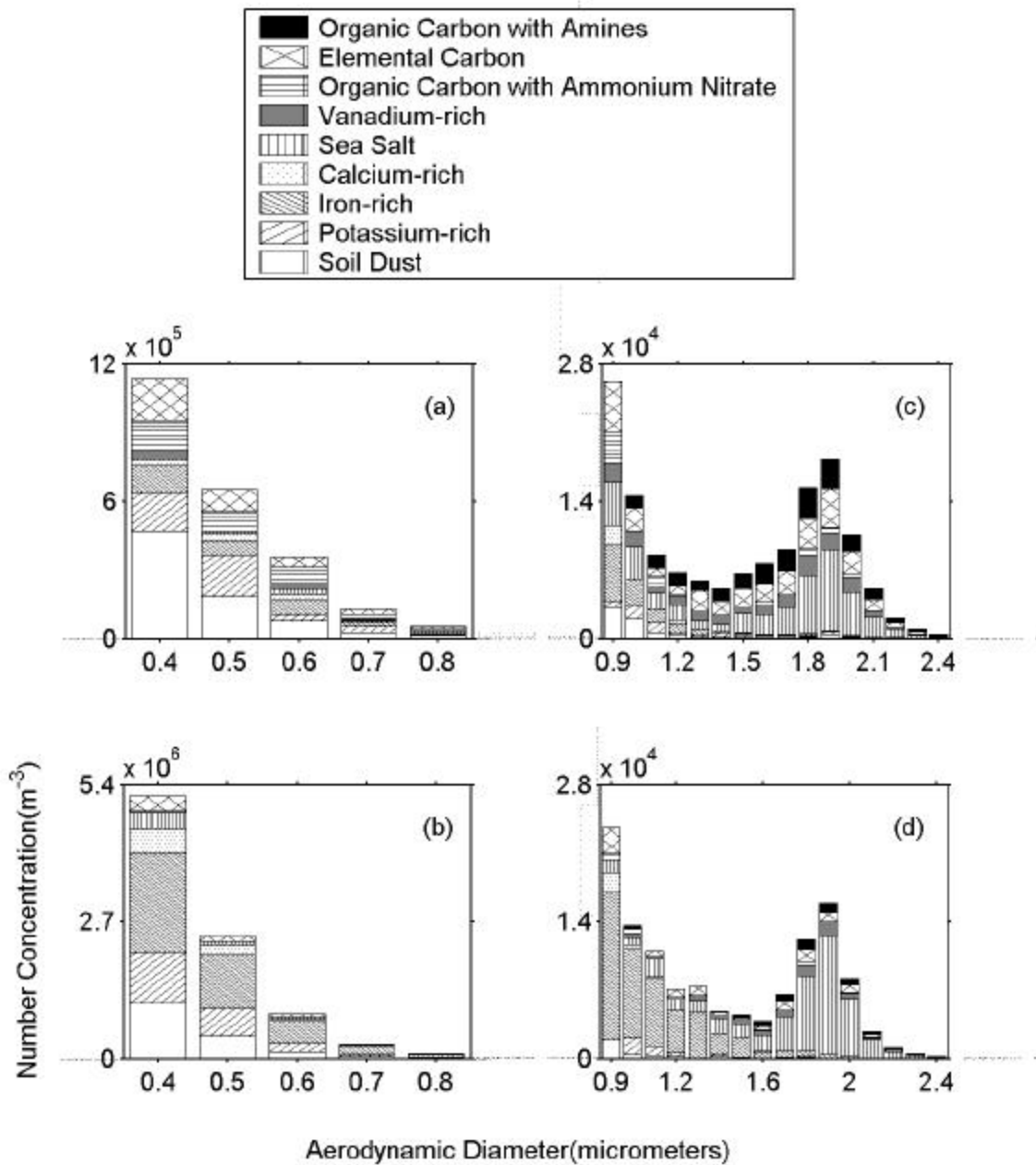


Figure 2.14: Scaled size distribution plots for Riverside, CA. Plots (a) and (c) represent morning periods of elevated PM<sub>10</sub> - an average of 6:30-7:30 August 21, 7:30-8:30 August 22, and 7:30-8:30 August 23, 1997. Plots (b) and (d) represent afternoon periods of elevated ozone - an average of 14:30-15:30 August 21, 16:30-17:30 August 22, and 12:30-13:30 August 23, 1997. Each bar is pattern coded for the general chemical composition.

## 2.4 Conclusions

This chapter provides details on the individual particle types present during August 21-23, 1997 in Riverside, CA, showing the temporal variations of the common particle types. A comparison of the particle types present during morning peaks of high  $PM_{10}$  and low ozone is made with afternoon periods with high ozone,  $PM_{10}$ , and  $b_{scat}$ . The particles were classified by ART-2a analysis, creating 57 classes. The top 20 classes, which represent more than eighty-five percent of the particles, are discussed in detail. The class types in Riverside, CA included organic carbon with amines, elemental carbon, organic carbon, ammonium nitrate, sea salt, soil dust, and various metal-rich types. The combination of ATOFMS to determine particle size and composition, and neural networks to classify those particles creates a powerful method for describing the ambient particle population and distinguishing differences in the particle population.

On August 21-23, 1997, two types of air pollution episodes, mornings with elevated  $PM_{10}$  and afternoons with elevated ozone, were shown to have different size distributions and were characterized by particles of different chemical composition. Inorganic particle types, super- $\mu m$  dust with some sea salt particles, characterized the morning episodes. Soil and other dust-type particles were particularly evident during the morning episodes on August 21 and 22. The afternoon episodes were characterized by the increased presence of sub- $\mu m$  carbon-rich particles, especially ammonium-nitrate-organic carbon particles which correlated with increased ozone levels. Sea salt and ammonium nitrate-organic particle types were anti-correlated throughout the study. The  $b_{scat}$  values tended to track the organic-ammonium nitrate particle types, particularly during the afternoon ozone events. Air parcel trajectories linked particle types to the air mass paths across the Los Angeles Basin, including a link between ammonium nitrate enriched organic carbon particle and stagnation near dairies in Mira Loma.

Opposing theories exist as to whether coarse ( $>2.5 \mu m$ ) or fine ( $<2.5 \mu m$ ) particles produce health effects (Brunekreef 2002). This is because during certain times, one size range of particles has been shown to produce a certain effect, while at other times this same size range of particles has shown no effect. These conflicting results are most likely due to the fact that at different times and locations, the size cut at  $PM_{2.5}$  does not separate compositions from different sources (i.e. coarse particles (i.e. dust, sea salt) from accumulation mode particles (i.e. combustion (organic)), and therefore cannot separate the effects due to fine and coarse particulate matter. Particles from such different sources have been shown to have quite different health effects (Laden 2000; Morawska 2002). This study confirms  $PM_{1.0}$  would be more effective at separating particles from these sources which produce drastically different compositions. This same size-composition trend has been shown previously in other ATOFMS studies conducted in other regions of the United States and world including the Indian Ocean (Guazzotti 2001), Atlanta (Liu 2003; Wenzel 2003), Texas, as well as bulk source combustion studies and ambient size distribution measurements (Kleeman 1999; Morawska 2002; Salma 2002). Based on these findings, in future health effects studies, using a cut-point at  $1 \mu m$  (as opposed to  $2.5 \mu m$ ) would most likely provide results which are less ambiguous and easier to interpret from day to day and location to location.